with either agent alone. Similarly, cell viabilities of KOB treated with 25 nM PS (LBH589), 2.5 μM DZNep, or a combination of these agents were 86%, 93%, and 48%, respectively. By calculating CI according to the method of Chou and Talalay,[29] we found a strong synergistic antiproliferative effect in both cell lines (*Online Supplementary Figure S5F*, lower panel).

Discussion

EZH2 is a critical component of PRC2, which mediates epigenetic gene silencing through trimethylation of H3K27.[37,38] EED and SUZ12 are also required for the exhibition of methyltransferase activity and for the localization of this complex to target genes.[39] In an analysis of genome-wide H3K27 methylation in aggressive prostate cancer tissues, a significant subset of the target genes were also targets in embryonic stem cells, suggesting that the mechanism for gene silencing used to maintain stem cell renewal is converted into oncogenesis.[40] Ectopic expression of EZH2 is capable of providing a proliferative advantage to primary cells, and its gene locus is amplified in primary tumors.[41] Indeed, increased EZH2 expression has been reported in several types of cancer cells, and its clinical significance is extensively studied in prostate cancer.[42] Amounts of both *EZH2* transcript and EZH2 protein were elevated in metastatic prostate cancer; in addition, clinically localized prostate cancers that express higher concentrations of *EZH2* showed a poorer prognosis. An association of increased EZH2 expression with poor prognosis has also been reported in other solid tumors. Currently, however, there are only limited reports describing EZH2 expression in hematologic malignancies.

In the present study, we showed for the first time that EZH2 was over-expressed in ATL cells, and that the increased EZH2 was not phosphorylated and was in its active form. The increased EZH2 seemed to exhibit histone methyltransferase activity *in vivo*, as supported by the results that ATL cells from both peripheral blood and lymph nodes were strongly positive for H3K27me3. Since EZH2 was almost undetectable in cells from healthy adults and HTLV-1 carriers, it is likely that deregulation of PRC2 caused by over-expressed EZH2 is involved in the early steps of ATL oncogenesis. Meanwhile, ATL patients with high EZH2 expression showed shorter survival than patients with low EZH2 expression, indicating that increased EZH2 also plays a role in the process of ATL progression. It has been reported that genes methylated in cancer cells are specifically packaged with nucleosomes containing H3K27.[43] However, there are only a few studies that actually examined H3K27me3 in primary tumor cells or tissues. In one such study, H3K27me3 expression was unexpectedly lower in breast, ovarian, and pancreatic cancers than in corresponding normal tissues, although it has been reported that there are increased levels of H3K27me3 in breast cancer cell lines.[44,45] We do not have an adequate explanation for these conflicts at present, but there may be some differences in the process of oncogenesis between solid tumors and hematologic malignancies.

The mechanism of the overexpression of EZH2 in tumors remains largely unknown. miRNAs regulate gene expression and play important roles in cellular differentiation and embryonic stem cell development. Recently, two miRNAs, miR-101 and miR-26a, were found to repress *EZH2* expression. The expression of miR-101 decreases in parallel with an increase in *EZH2* expression during progression in prostate tumors.[34] In addition to these miRNAs, we examined miR-128a, which has been shown to repress *BMI1* expression in glioblastoma, because overexpression of *BMI-1* is associated with the development of malignant lymphoma.[31,36] ATL cells showed a decreased level of miR-

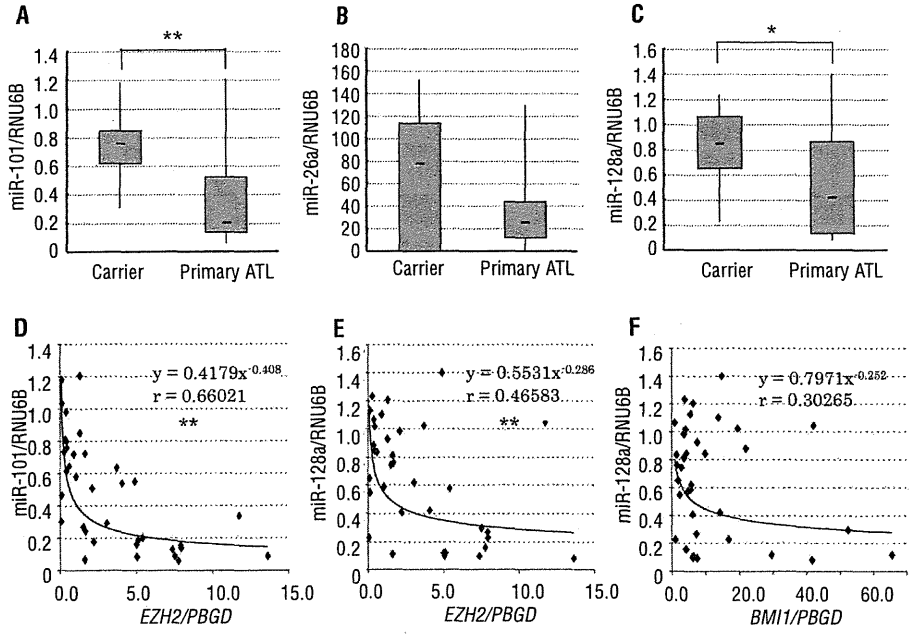

Figure 3. Quantitative real-time RT-PCR for miRNAs. (A-C) Expressions of miR-101 (A), miR-26a (B), and miR-128a (C) were compared between ATL patients and HTLV-1 carriers. Primary ATL cells showed significantly lower levels of miR-101 and miR-128a (Mann-Whitney's U test) compared with the cells from HTLV-1 carriers (A, C). There was no significant difference in miR-26a expression between the two groups (B). (D, E, F) Correlation between miRNA and *EZH2* or *BMI1* expression was examined. There were significant inverse correlations between normalized *EZH2* expression and miR-101 expression (D) or between normalized *EZH2* expression and miR-128a expression (E) (Spearman's correlation coefficient). In contrast, there was no correlation between normalized *BMI1* expression and miR-128a expression (F). *$P<0.05$, **$P<0.01$

101 expression compared with the cells from HTLV-1 carriers, which is not caused by genomic loss of the *miR-101* gene, in contrast to prostate cancer.[34] Moreover, there was a clear inverse correlation between *EZH2* expression and miR-101 expression, suggesting that increased *EZH2* is caused by the decrease in miR-101 expression. Although currently there is no report indicating an association of miR-128a with *EZH2* expression, miR-128a showed exactly the same pattern as miR-101, suggesting that the decrease in miR-128a also participates in *EZH2* overexpression in ATL. By analyzing the 3'-UTR sequence of *EZH2*, it has recently been shown that there are two predicted miR-101 target sites and one predicted miR-26a target site in the 3'-UTR of EZH2.[46] We performed a similar analysis and found that there was also a potential target site for miR-128a near one of the miR-101 target sites (*Online Supplementary Figure S6*). miR-26a was not decreased in ATL cells, and there was no correlation between miR-26a expression and *EZH2* expression or miR-128a expression and *BMI1* expression. The association of miR-26a with *EZH2* was found in normal cell differentiation as a physiological phenomenon but not in tumor cells. The miRNAs used to regulate normal development and differentiation may be different from those used for the development of tumors. Another possible explanation for the mechanism of increased *EZH2* expression in ATL is inactivation of *p14ARF/p15INK4B/p16INK4A* tumor suppressor genes, which frequently occurs in ATL.[14,15,19,20] EZH2 is a mólecule downstream of the pRB-E2F pathway, and inactivation of these genes allows E2F to be released from pRB, which results in the upregulation of *EZH2* expression.[41] Several recent reports indicate that EZH2 functions to repress the expression of *p14ARF/p15INK4B/p16INK4A*; therefore, increased EZH2 may be used to further decrease the expression of *p14ARF/p15INK4B/p16INK4A*.[47] Since somatic mutations altering EZH2 (Tyr641) have recently been reported in follicular and diffuse large B-cell lymphomas of germinal-center origin,[48] we performed a similar analysis in 10 primary ATL samples. There were however no such mutations (*Online Supplementary Figure S7*).

ATL is quite resistant to antineoplastic agents and the median survival time of those with the aggressive subtypes is only 13 months, even in a recent multicenter clinical trial.[49] Since high EZH2 expression with H3K27me3 seems to be an essential component for the initiation and promotion of cell proliferation in ATL, we searched for the possibility of therapeutic strategies targeting EZH2. We examined the sensitivity of ATL cells to agents that have been shown to inhibit *EZH2* expression and histone methylation. DZNep is a carbocyclic analog of adenosine synthesized more than 20 years ago as an inhibitor of S-adenosylhomocysteine hydrolase, which has therapeutic potential as an anticancer or antiviral drug.[21] DZNep has recently aroused interest for its unique features; it decreases the expressions of *EZH2*, *SUZ12*, and *EED* with inhibition of H3K27 methylation and induces apoptosis in cancer cells but not in normal cells.[22,23] ATL cell lines were sensitive to DZNep and their cell proliferation was attenuated at one-tenth of the concentration used in these studies. More interestingly, DZNep showed no toxicity to normal $CD4^+$ T cells as a normal control. Acute T-lymphoblastic leukemia cell lines showed similar sensitivities to DZNep, which may indicate that DZNep exerts general toxicity to leukemia and lymphoma cells not necessarily associated with histone modification. Indeed, although DZNep rather increased EZH2 expression in KOB cells, this cell line was equally sensitive as other cell lines to DZNep. HDAC inhibitor PS (LBH589) is an effective agent for cutaneous T-cell lymphoma and induced complete remission in 2 of 9 patients involved in a phase I clinical trial.[50] More interestingly, it has been reported recently that combined use of DZNep and PS (LBH589) yielded more depletion of EZH2 and induced more apoptosis of leukemia cells, but not normal CD34 (+) bone marrow progenitor cells.[51] In the present study, we showed that the combination of DZNep and PS (LBH589) exhibited a synergistic effect in killing ATL cells. Thus, epigenetic therapy by the combined use of these agents that inhibit histone methylation could lead to a breakthrough in the treatment of aggressive ATL.

Authorship and Disclosures

The information provided by the authors about contributions from persons listed as authors and in acknowledgments is available with the full text of this paper at www.haematologica.org.

Financial and other disclosures provided by the authors using the ICMJE (www.icmje.org) Uniform Format for Disclosure of Competing Interests are also available at www.haematologica.org.

References

1. Sparmann A, van Lohuizen M. Polycomb silencers control cell fate, development and cancer. Nat Rev Cancer. 2006;6(11):846-56.
2. Lee TI, Jenner RG, Boyer LA, Guenther MG, Levine SS, Kumar RM, et al. Control of developmental regulators by Polycomb in human embryonic stem cells. Cell. 2006;125(2):301-13.
3. Kamminga LM, Bystrykh LV, de Boer A, Houwer S, Douma J, Weersing E, et al. The Polycomb group gene Ezh2 prevents hematopoietic stem cell exhaustion. Blood. 2006;107(5):2170-9.
4. van Lohuizen M, Tijms M, Voncken JW, Schumacher A, Magnuson T, Wientjens E. Interaction of mouse polycomb-group (Pc-G) proteins Enx1 and Enx2 with Eed: Indication for separate Pc-G complexes. Mol Cell Biol. 1998;18(6):3572-9.
5. Satijn DP, Hamer KM, den Blaauwen J, Otte AP. The Polycomb group protein EED interacts with YY1, and both proteins induce neural tissue in Xenopus embryos. Mol Cell Biol. 2001;21(4):1360-9.
6. van der Vlag J, Otte AP. Transcriptional repression mediated by the human polycomb-group protein EED involves histone deacetylation. Nat Genet. 1999;23(4):474-8.
7. Vire E, Brenner C, Deplus R, Blanchon L, Fraga M, Didelot C, et al. The Polycomb group protein EZH2 directly controls DNA methylation. Nature. 2006;439(7078):871-4.
8. Cao R, Zhang Y. The functions of E(Z)EZH2-mediated methylation of lysine 27 in histoneH3. Curr Opin Genet Dev. 2004;14(2):155-64.
9. Widschwendter M, Fiegl H, Egle D, Mueller-Holzner E, Spizzo G, Marth C, et al. Epigenetic stem cell signature in cancer. Nat Genet. 2007;39(2):157-8.
10. Simon JA, Lange CA. Roles of the EZH2 histone methyltransferase in cancer epigenetics. Mutat Res. 2008;647(1-2):21-9.
11. Uchiyama T, Yodoi J, Sagawa K, Takatsuki K, Uchino H. Adult T-cell leukemia: clinical and hematologic features of 16 cases. Blood. 1977;50(3):481-92.
12. Yoshida M, Seiki M, Yamaguchi K, Takatsuki K. Monoclonal integration of human T-cell leukemia provirus in all primary tumors of adult T-cell leukemia suggests causative role of human T-cell leukemia virus in the disease. Proc Natl Acad Sci USA. 1984;81(8):2534-7.
13. Shimoyama M and members of the Lymphoma Study Group (1984-1987):

Diagnostic criteria and classification of clinical subtypes of adult T-cell leukaemia-lymphoma. A report from the Lymphoma Study Group (1984-1987). Br J Haematol. 1991;79(3):428-37.
14. Hatta Y, Hirama T, Miller CW, Yamada Y, Tomonaga M, Koeffler HP. Homozygous deletions of p15 (MTS2) and p16 (CDKN2/MTS1) genes in adult T-cell leukemia. Blood. 1995;85(10):2699-704.
15. Yamada Y, Hatta Y, Murata K, Sugawara K, Ikeda S, Mine M, et al. Deletions of p15 and/or p16 genes as a poor-prognosis factor in adult T-cell leukemia. J Clin Oncol. 1997;15(5):1778-85.
16. Nagai H, Kinoshita T, Imamura J, Murakami Y, Hayashi K, Mukai K, et al. Genetic alteration of p53 in some patients with adult T-cell leukemia. Jpn J Cancer Res. 1991;82(12):1421-7.
17. Sakashita A, Hattori T, Miller CW, Suzushima H, Asou N, Takatsuki K, et al. Mutations of the p53 gene in adult T-cell leukemia. Blood. 1992;79(2):477-80.
18. Tawara M, Hogerzeil SJ, Yamada Y, Takasaki Y, Soda H, Hasegawa H, et al. Impact of p53 aberration on the progression of adult T-cell leukemia/lymphoma. Cancer Lett. 2006;234(2):249-55.
19. Kohno T, Yamada Y, Tawara M, Takasaki Y, Kamihira S, Tomonaga M, et al. Inactivation of p14ARF as a key event for the progression of adult T-cell leukemia/lymphoma. Leuk Res. 2007;31(12):1625-32.
20. Nosaka K, Maeda M, Tamiya S, Sakai T, Mitsuya H, Matsuoka M. Increasing methylation of the CDKN2A gene is associated with the progression of adult T-cell leukemia. Cancer Res. 2000;60(4):1043-8.
21. Glazer RI, Hartman KD, Knode MC, Richard MM, Chiang PK, Tseng CK, et al. 3-Deazaneplanocin: a new and potent inhibitor of S-adenosylhomocysteine hydrolase and its effects on human promyelocytic leukemia cell line HL-60. Biochem Biophys Res Commun. 1986;135 (2):688-94.
22. Miranda TB, Cortez CC, Yoo CB, Liang G, Abe M, Kelly TK, et al. DZNep is a global histone methylation inhibitor that reactivates developmental genes not silenced by DNA methylation. Mol Cancer Ther. 2009;8(6):1579-88.
23. Tan J, Yang X, Zhuang L, Jiang X, Chen W, Lee PL, et al. Pharmacologic disruption of Polycomb-repressive complex 2-mediated gene repression selectively induces apoptosis in cancer cells. Genes Dev. 2007;21(9): 1050-63.
24. Fiskus W, Pranpat M, Balasis M, Herger B, Rao R, Chinniyan A, et al. Histone deacetylase inhibitors deplete EZH2 and associated Polycomb Repressive Complex 2 proteins with attenuation of HOXA9 and MEIS1 and loss of survival of human acute leukemia cells. Mol Cancer Ther. 2006;5 (12):3096-104.
25. Choi YL, Tsukasaki K, O'Neill MC, Yamada Y, Onimaru Y, Matsumoto K, et al. A genomic analysis of adult T-cell leukemia. Oncogene. 2007;26(8):1245-55.
26. Yamada Y, Ohmoto Y, Hata T, Yamamura M, Murata K, Tsukasaki K, et al. Features of the cytokines secreted by adult T cell leukemia (ATL) cells. Leuk Lymphoma. 1996;21(5-6):443-7.
27. Choi YL, Makishima H, Ohashi J, Yamashita Y, Ohki R, Koinuma K, et al. DNA microarray analysis of natural killer cell-type lymphoproliferative disease of granular lymphocytes with purified CD3(-) CD56(+) fractions. Leukemia. 2004;18(3): 556-65.
28. Hasegawa H, Yamada Y, Komiyama K, Hayashi M, Ishibashi M, Sunazuka T, et al. A novel natural compound, a cycloanthranilylproline derivative (Fuligocandin B), sensitizes leukemia cells to apoptosis induced by tumor necrosis factor related apoptosis-inducing ligand (TRAIL) through 15-deoxy-Delta 12, 14 prostaglandin J2 production. Blood. 2007;110(5):1664-74.
29. Chou TC, Talalay P. Quantitative analysis of dose-effect relationships: the combined effects of multiple drugs or enzyme inhibitors. Adv Enzyme Regul. 1984;22:27-55.
30. Yasunaga J, Taniguchi Y, Nosaka K, Yoshida M, Satou Y, Sakai T, et al. Identification of aberrantly methylated genes in association with adult T-cell leukemia. Cancer Res. 2004;64(17):6002-9.
31. Jacobs JJ, Kieboom K, Marino S, DePinho RA, van Lohuizen M. The oncogene and Polycomb-group gene bmi-1 regulates cell proliferation and senescence through the ink4a locus. Nature. 1999;397(6715):164-8.
32. Scott CL, Gil J, Hernando E, Teruya-Feldstein J, Narita M, Martinez D, et al. Role of the chromobox protein CBX7 in lymphomagenesis. Proc Natl Acad Sci USA. 2007;104(13):5389-94.
33. Cha TL, Zhou BP, Xia W, Wu Y, Yang CC, Chen CT, et al. Akt-mediated phosphorylation of EZH2 suppresses methylation of Lysine 27 in histone H3. Science. 2005;310(5746):306-10.
34. Varambally S, Cao Q, Mani RS, Shankar S, Wang X, Ateeq B, et al. Genomic loss of microRNA-101 leads to overexpression of histone methyltransferase EZH2 in cancer. Science. 2008;322(5908):1695-6.
35. Sander S, Bullinger L, Klapproth K, Fiedler K, Kestler HA, Barth TF, et al. MYC stimulates EZH2 expression by repression of its negative regulator miR-26a. Blood. 2008; 112(10):4202-12.
36. Godlewski J, Nowicki MO, Bronisz A, Williams S, Otsuki A, Nuovo G, et al. Targeting of the Bmi-1 oncogene/stem cell renewal factor by microRNA-128 inhibits glioma proliferation and self-renewal. Cancer Res. 2008;68(22):9125-30.
37. Cao R, Wang L, Wang H, Xia L, Erdjument-Bromage H, Tempst P, et al. Role of histone H3 lysine 27 methylation in Polycomb-group silencing. Science. 2002;298(5595): 1039-43.
38. Czermin B, Melfi R, McCabe D, Seitz V, Imhof A, Pirrotta V. Drosophila enhancer of Zeste/ESC complexes have a histone H3 methyltransferase activity that marks chromosomal Polycomb sites. Cell. 2002;111(2): 185-96.
39. Cao R, Zhang YI. SUZ12 is required for both the histone methyltransferase activity and the silencing function of the EED-EZH2 complex. Mol Cell. 2004;15(1):57-67.
40. Yu J, Yu J, Rhodes DR, Tomlins SA, Cao X, Chen G, et al. A polycomb repression signature in metastatic prostate cancer predicts cancer outcome. Cancer Res. 2007; 67(22):10657-63.
41. Bracken AP, Pasini D, Capra M, Prosperini E, Colli E, Helin K. EZH2 is down stream of the pRB-E2F pathway, essential for proliferation and amplified in cancer. EMBO J. 2003;22(20):5323-35.
42. Varambally S, Dhanasekaran SM, Zhou M, Barrette TR, Kumar-Sinha C, Sanda MG, et al. The polycomb group protein EZH2 is involved in progression of prostate cancer. Nature. 2002;419(6907):624-9.
43. Schlesinger Y, Straussman R, Keshet I, Farkash S, Hecht M, Zimmerman J, et al. Polycomb-mediated methylation of Lys27 of histone H3 pre-marks genes for de novo methylation in cancer. Nat Genet. 2007;39 (2):232-6.
44. Wei Y, Xia W, Zhang Z, Liu J, Wang H, Adsay NV, et al. Loss of trimethylation at lysine 27 of histone H3 is a predictor of poor outcome in breast, ovarian, and pancreatic cancers. Mol Carcinog. 2008;47 (9):701-6.
45. Sun F, Chan E, Wu Z, Yang X, Marquez VE, Yu Q. Combinatorial pharmacologic approaches target EZH2-mediated gene repression in breast cancer cells. Mol Cancer Ther. 2009;8(12):3191-202.
46. Cao P, Deng Z, Wan M, Huang W, Cramer SD, Xu J, et al. MicroRNA-101 negatively regulates Ezh2 and its expression is modulated by androgen receptor and HIF-1alpha/HIF-1beta. Mol Cancer. 2010;9: 108.
47. Bracken AP, Kleine-Kohlbrecher D, Dietrich N, Pasini D, Gargiulo G, Beekman C, et al. The polycomb group proteins bind throughout the INK4A-ARF locus and are disassociated in senescent cells. Genes Dev. 2007;21(5):525-30.
48. Morin RD, Johnson NA, Severson TM, Mungall AJ, An J, Goya R, et al. Somatic mutations altering EZH2 (Tyr641) in follicular and diffuse large B-cell lymphomas of germinal-center origin. Nat Genet. 2010; 42(2):181-5.
49. Yamada Y, Tomonaga M, Fukuda H, Hanada S, Utsunomiya A, Tara M, et al. A new G-CSF-supported combination chemotherapy, LSG15, for adult T-cell leukaemia-lymphoma: Japan Clinical Oncology Group Study 9303. Br J Haematol. 2001;113(2):375-82.
50. Ellis L, Pan Y, Smyth GK, George DJ, McCormack C, Williams-Truax R, et al. Histone deacetylase inhibitor panobinostat induces clinical responses with associated alterations in gene expression profiles in cutaneous T-cell lymphoma. Clin Cancer Res. 2008;14(14):4500-10.
51. Fiskus W, Wang Y, Sreekumar A, Buckley KM, Shi H, Jillella A, et al. Combined epigenetic therapy with the histone methyltransferase EZH2 inhibitor 3-deazaneplanocin A and the histone deacetylase inhibitor panobinostat against human AML cells. Blood. 2009;114(13):2733-43.

blood

2011 118: 6881-6892
Prepublished online October 31, 2011;
doi:10.1182/blood-2011-05-354654

miR-135b mediates NPM-ALK–driven oncogenicity and renders IL-17–producing immunophenotype to anaplastic large cell lymphoma

Hironori Matsuyama, Hiroshi I. Suzuki, Hikaru Nishimori, Masaaki Noguchi, Takashi Yao, Norio Komatsu, Hiroyuki Mano, Koichi Sugimoto and Kohei Miyazono

Blood (print ISSN 0006-4971, online ISSN 1528-0020), is published weekly by the American Society of Hematology, 2021 L St, NW, Suite 900, Washington DC 20036.

miR-135b mediates NPM-ALK–driven oncogenicity and renders IL-17–producing immunophenotype to anaplastic large cell lymphoma

*Hironori Matsuyama,[1] *Hiroshi I. Suzuki,[1] Hikaru Nishimori,[1] Masaaki Noguchi,[2] Takashi Yao,[3] Norio Komatsu,[4] Hiroyuki Mano,[5,6] Koichi Sugimoto,[4] and Kohei Miyazono[1]

[1]Department of Molecular Pathology, Graduate School of Medicine, University of Tokyo, Tokyo, Japan; [2]Department of Hematology, Juntendo Urayasu Hospital, Chiba, Japan; [3]Department of Human Pathology and [4]Division of Hematology, Department of Internal Medicine, Juntendo University School of Medicine, Tokyo, Japan; [5]Department of Medical Genomics, Graduate School of Medicine, University of Tokyo, Tokyo, Japan; and [6]Division of Functional Genomics, Jichi Medical University, Tochigi, Japan

Many transformed lymphoma cells show immune-phenotypes resembling the corresponding normal lymphocytes; thus, they provide a guide for proper diagnosis and present promising routes to improve their pathophysiologic understanding and to identify novel therapeutic targets. However, the underlying molecular mechanism(s) of these aberrant immune-phenotypes is largely unknown. Here, we report that microRNA-135b (miR-135b) mediates nucleophosmin-anaplastic lymphoma kinase (NPM-ALK)–driven oncogenicity and empowers IL-17–producing immunophenotype in anaplastic large cell lymphoma (ALCL). NPM-ALK oncogene strongly promoted the expression of miR-135b and its host gene LEMD1 through activation of signal transducer and activator of transcription (STAT) 3. In turn, elevated miR-135b targeted FOXO1 in ALCL cells. miR-135b introduction also decreased chemosensitivity in Jurkat cells, suggesting its contribution to oncogenic activities of NPM-ALK. Interestingly, miR-135b suppressed T-helper (Th) 2 master regulators STAT6 and GATA3, and miR-135b blockade attenuated IL-17 production and paracrine inflammatory response by ALCL cells, indicating that miR-135b–mediated Th2 suppression may lead to the skewing to ALCL immunophenotype overlapping with Th17 cells. Furthermore, antisense-based miR-135b inhibition reduced tumor angiogenesis and growth in vivo, demonstrating significance of this "Th17 mimic" pathway as a therapeutic target. These results collectively illuminated unique contribution of oncogenic kinase-linked microRNA to tumorigenesis through modulation of tumor immune-phenotype and microenvironment. (*Blood.* 2011;118(26):6881-6892)

Introduction

MicroRNAs (miRNAs) are endogenous noncoding, 20- to 23-nucleotide single-stranded RNAs that negatively regulate gene expression in a sequence-specific manner.[1] miRNA species are generated through RNase-mediated processing reaction by two central RNases III, Drosha and Dicer, from long primary transcripts (primary miRNAs [pri-miRNAs]) and incorporated along with core Argonaute proteins into the RNA-induced silencing complex. RNA-induced silencing complex interacts mainly with 3′ untranslated region (UTR) of target mRNAs through partial base complementarity to the 5′ miRNA seed region, leading to degradation, destabilization, or translational inhibition of target mRNAs. miRNAs regulate differentiation and functions of various cell types, including immune cells in a highly context-dependent manner.[2]

Alteration of miRNome has emerged as a key feature of cancer-associated dysfunction of gene regulatory networks. Although miRNA dysregulation affects cancer cell behavior with other genetic and epigenetic abnormalities, full pictures of their causes and consequences remain to be elucidated.[3] In hematologic malignancies, many transformed lymphoma cells show immune-phenotypes resembling the corresponding normal lymphocytes; thus, they represent a guide for proper diagnosis and promising routes to improve our understanding of their pathogenesis and to identify novel therapeutic targets.[4] For example, diffuse large B-cell lymphomas have been shown to be composed of at least 2 prognostic entities, depending on its resemblance to normal germinal center or activated B cells.[5] However, the molecular basis shaping the aberrant immunophenotypes of tumor cells has been largely unknown, and the relationship between miRNA regulation and lymphoma phenotype has not been investigated.

Recent studies revealed several mechanisms regulating miRNA expression.[6] Although certain oncoproteins, including Myc and tumor suppressors such as p53, have been linked to the regulation of miRNA expression,[7,8] involvement of oncogenic tyrosine kinases remains unclear in this regulatory pathway. Anaplastic lymphoma kinase (ALK) exerts characteristic oncogenic activities through fusion to several gene partners or mutations both in hematopoietic and nonhematopoietic solid tumors.[9,10] Nucleophosmin (NPM)–ALK is a representative translocation-dependent fusion-type oncogenic tyrosine kinase in anaplastic large cell lymphoma (ALCL). Although NPM-ALK drives malignant transformation of ALCL cells through various molecular mechanisms, including activation of signal transducer and activator of transcription (STAT) 3, Ras-ERK, and PI3K oncogenic signaling pathways,[9] involvement of miRNAs has not been reported so far. Here, we have explored unrecognized involvement of miRNAs in the downstream of NPM-ALK.

Submitted May 12, 2011; accepted October 25, 2011. Prepublished online as *Blood* First Edition paper, October 31, 2011; DOI 10.1182/blood-2011-05-354654.

*H.M. and H.I.S. contributed equally to this study.

The online version of the article contains a data supplement.

The publication costs of this article were defrayed in part by page charge payment. Therefore, and solely to indicate this fact, this article is hereby marked "advertisement" in accordance with 18 USC section 1734.

We identified miR-135b as one of the major downstream executors of NPM-ALK chimeric oncoprotein in ALCL. NPM-ALK strongly promoted the expression of miR-135b and its host gene LEMD1 through STAT3 activation. The elevated miR-135b targeted FOXO1 tumor suppressor. Interestingly, we further revealed the immune modulatory property of miR-135b shaping the T-cell phenotypes of ALCL cells. miR-135b suppressed T-helper (Th) 2 master regulators STAT6 and GATA3, and the blockade of miR-135b attenuated IL-17 production and paracrine inflammatory response by ALCL cells, suggesting that miR-135b–mediated Th2 suppression may skew the ALCL immunophenotype to overlap with that of Th17 cells. Antisense-based miR-135b inhibition reduced tumor angiogenesis and growth in vivo, underscoring the pathogenic roles of this pathway. Our findings revealed that miR-135b is involved in NPM-ALK–driven tumorigenesis and modulation of ALCL immunophenotype, and they also suggest dynamic commitment of miRNAs to mutual regulation between Th cell differentiation programs and determination of polarized immunophenotypes of malignant cells.

Methods

Cell lines and reagents

Karpas 299, SUDHL-1, and SUP-M2 cell lines were obtained from the German Collection of Microorganisms and Cell Cultures. Jurkat, Molt4, CCRF-CEM, HCT116, HEK293T, HeLa, and lung cancer cell lines were obtained from the American Type Culture Collection. WI-38 human diploid fibroblast line was obtained from the RIKEN Cell Bank. Human normal peripheral blood pan T lymphocytes were purchased from AllCells. Neuroblastoma cell lines were kindly provided from R. Sakai (National Cancer Center Research Institute, Tokyo, Japan). Hematologic, neuroblastoma, and lung cancer cell lines were maintained in RPMI-1640 (Invitrogen) containing 10% FBS, 100 units/mL penicillin, and 100 μg/mL streptomycin. Other cell lines were maintained in Dulbecco modified eagle medium (Invitrogen) with 10% FBS. In coculture experiment, Karpas 299 and WI-38 cells were cocultured (in Opti-MEM [Invitrogen] with 1% FBS) for 48 hours using Transwell tissue culture inserts (0.4-μm pore size; BD Biosciences). The following antibodies were used: ALK 4C5B8 (Invitrogen); STAT3 124H6, p-STAT3 D3A7, Akt 9272, p-Akt 193H12, FOXO1 C29H4, and STAT6 9362 (Cell Signaling Technology); p21 H-164, p27 F-8, and GATA3 HG3-31 (Santa Cruz Biotechnology); CREG1 299133 (R&D Systems); CD31 555024 (BD Biosciences); and α-tubulin DM-1A (Sigma-Aldrich). Kinase inhibitors (WHI-P154, U0126 and LY294002) were purchased from Calbiochem.

Patient samples

ALCL patients were diagnosed at Juntendo University Hospital and Juntendo Urayasu Hospital. Investigations were carried out in accordance with ethical standards authorized by the ethics committees of University of Tokyo, Juntendo University School of Medicine, and Jichi Medical University. Written informed consent was obtained in accordance with the Declaration of Helsinki.

TuD miRNA system, shRNA, and plasmids

Tough decoy RNA (TuD RNA) against miR-135b was designed according to a previous report.[11] Detailed structures of TuD RNA are described in supplemental Table 1 (available on the *Blood* Web site; see the Supplemental Materials link at the top of the online article). shRNAs were designed as described previously.[12,13] TuD RNAs and shRNAs were introduced into pENTR-H1 vector. Pri-miRNA expression vectors were generated by cloning short fragments of pri-miRNAs containing pre-miRNA and flanking sequence on both sides of pre-miRNA into pcDNA6.2-GW/EmGFP-miR (Invitrogen). miRNA sensor vectors were prepared by inserting mature miRNA complementary sequences within the XhoI and NotI sites of the 3′UTR of the luciferase gene in the Psicheck 2 dual luciferase reporter vector (Promega). For other reporter constructs, the 3′UTR segment of each target gene was cloned into the same luciferase reporter vector. The primer sequences used are given in supplemental Table 2. For transient transfection, pre-miR miRNA precursors (Ambion) also were used.

Luciferase reporter assay

Cells were transfected with each reporter construct with pri-miRNA expression vector using Lipofectamine 2000 (Invitrogen). Cell extracts were prepared 24 to 48 hours after transfection, and the ratio of *Renilla* to firefly luciferase was measured using the Dual-Luciferase Reporter Assay System (Promega).

qRT-PCR assays

Quantitative (q)RT-PCR assays were performed as described previously.[8] For detection of mRNAs, total RNA was extracted by TRIzol (Invitrogen) and subjected to reverse transcription using the PrimeScriptII first-strand cDNA synthesis kit (Takara) according to the manufacturer's instructions. qRT-PCR was performed with the 7500 Fast Real-Time PCR System (Applied Biosystems). The expression levels of mature miRNAs were determined using TaqMan MicroRNA assay kit (Applied Biosystems) according to the manufacturer's protocol. Data analysis was done by the comparative C_T method. Results were normalized to β-actin for pri-miRNA detection, and RNU44 small nucleolar RNA for evaluation of mature miRNA. miRNeasy mini kit (QIAGEN) or RecoverAll total nucleic acid isolation kit for FFPE Tissues (Ambion) was used for RNA extraction from clinical samples. The primer sequences used are given in supplemental Table 3.

Chromatin immunoprecipitation analysis

Cells were fixed by adding formaldehyde and then harvested. After sonication, samples were incubated at 4°C overnight with protein A or anti–mouse IgG-Dynabeads that had been preincubated with 5 to 10 μg of antibodies in PBS and 0.5% BSA. To precipitate STAT3, anti-STAT3 antibody 124H6 (Cell Signaling Technology) was used. Immunoprecipitated samples were eluted and reverse-crosslinked by incubation overnight at 65°C. Genomic DNA was then extracted with a PCR purification kit (QIAGEN) and subjected to PCR analysis. The primer sequences used are given in supplemental Table 3.

Lentiviral gene transfer

TuD RNAs, shRNAs, pri-miRNA, NPM-ALK, or mouse constitutively active (ca)–STAT3 (A662C/N664C)[14] was introduced by lentiviral infection system (a kind gift from H. Miyoshi, RIKEN, Tsukuba, Japan). TuD RNAs and shRNAs were transferred into lentivirus vector CS-RfA-EG via pENTR-H1 vector using LR clonase. Pri-miRNA was similarly transferred into CSII-EF-RfA-CMV-Puro lentivirus vector using pENTR vector. The lentivirus production was carried out by transfection of HEK293FT cells with the vector construct pCMV-VSV-G-RSV-Rev and pCAG-HIVgp. The viral particles were collected 48 hours after transfection, titered by Lenti-X qRT-PCR titration kit (Takara), introduced to cultured cells, and monitored by flow cytometric analysis to determine infection efficiency.

Immunoblot assay

Cells were lysed with a buffer containing 1% Nonidet P-40, 20mM Tris-HCl, pH 7.4, 150mM NaCl, 5mM EDTA, and 1% protease inhibitor mixture (Nacalai Tesque). Total cell lysates were subjected to SDS-PAGE and transferred to Fluoro Trans W membrane (Pall). Immunoblotting was performed using the indicated antibodies.

Drug sensitivity assay

Jurkat cells were seeded at a density of 1×10^5/mL and split 24 hours before treatment. After 24-hour treatment with different concentrations of cytosine β-D-arabinofuranoside (Sigma-Aldrich), cells were collected,

washed, and reseeded for assay of cell viability and apoptosis. Cell viability and apoptosis were assessed by WST-8 colorimetric assay (Nacalai Tesque) and annexin V assay kit (BD Biosciences), respectively.

ELISA

After transfection with miRCURY LNA microRNA power inhibitor (EXIQON; Control A or antisense against miR-135b), IL-17F concentrations in the culture supernatant (72 hours) of Karpas 299 cells were determined by ELISA kit (R&D Systems; Duoset human IL17F), according to the manufacturer's instructions.

In vivo cancer models

C.B-17/IcrCrj severe combined immunodeficient (SCID) female mice (4 weeks of age) were obtained from Charles River Japan. All animal experimental protocols were performed in accordance with the policies of the Animal Ethics Committee of the University of Tokyo. Karpas 299 cells (1×10^6; n = 6/group) were subcutaneously injected in 0.2 mL of a mixture of RPMI-1640 without FBS and 30% Matrigel (BD Biosciences) into female SCID mice and allowed to grow for 1 week to reach a volume of 50 to 200 mm^3. Complexes of miRCURY LNA microRNA power inhibitor (EXIQON; Control A or antisense against miR-135b) and atelocollagen (Koken) were prepared according to the manufacturer's instructions. Antisense oligonucleotides (5μM) with atelocollagen in a 200-μL volume were administered into the subcutaneous spaces around the tumors at days 7 and 10 after inoculation. Subcutaneous xenografts were measured externally every day until the end of evaluation periods, and tumor volume was approximated using the equation vol = $(a \times b^2)/2$, where vol is volume, a the length of the major axis, and b the length of the minor axis.

Immunohistochemistry

Tumor samples excised from the animals were fixed for 1 hour in 10% neutral-buffered formalin at room temperature, washed overnight in PBS containing 10% sucrose at 4°C, and embedded in optimal cutting temperature compound (Tissue-Tek). The samples were then snap-frozen in dry-iced acetone for immunohistochemistry. Frozen samples were further sectioned at 10-μm thickness in a cryostat, briefly fixed with 10% formalin, and then incubated with primary and secondary antibodies. Samples were observed using an LSM510 Meta confocal microscope (Carl Zeiss). Quantification of CD31-stained areas was performed in multiple fields on tumor sections from 6 mice using Photoshop 8.0.1 software (Adobe Systems) and ImageJ 1.36b software (National Institutes of Health).

GEP analysis

Microarray data for NPM-ALK gene expression signature (GSE6184) and clinical gene expression profiling (GEP) data of peripheral T-cell lymphoma (PTCL) patient samples (GSE19069) were obtained from the National Center for Biotechnology Information's Gene Expression Omnibus.[12,15] Gene-set enrichment analysis (GSEA) was performed with GSEA Version 2.0 software available from the Broad Institute (http://www.broadinstitute.org/gsea/) using microarray data for NPM-ALK signature (GSE6184) and GSEA-embedded potential miRNA target gene sets or TargetScan-predicted putative miRNA target lists (http://www.targetscan.org/).[16]

Statistical analysis

Statistical analysis was performed using the Student t test or multivariate ANOVA (for proliferation assay and in vivo analysis; $^*P < .05$; $^{**}P < .01$; $^{***}P < .001$). All data are expressed as mean ± SEM.

Results

Up-regulation of miR-135b in ALCL

Previous microarray analysis on miRNA expression identified various signatures of aberrant miRNA expression in a wide range of hematologic cell lines, including major types of B- and T-cell lymphoma, lymphoproliferative disorder, T-cell acute lymphoblastic leukemia, and acute myeloid leukemia.[17] In this analysis, ALCL was characterized by increased expression of miR-135b, miR-21, and miR-27a.[17] We verified the observation using quantitative RT-PCR analysis on 3 ALCL cell lines carrying *NPM-ALK* fusion; Karpas 299, SUDHL-1, and SUP-M2 (Figure 1A-C). Among these miRNAs, miR-135b was most prominently up-regulated in ALCL cell lines, and it was reduced by the ALK inhibitor WHI-P154 (Figure 1D), prompting us to track potential downstream effector(s) of NPM-ALK to miR-135b. Because miR-135b is located in the first intron of the LEM domain containing 1 (*LEMD1*) gene on 1q32.1 (Figure 1E), we examined LEMD1 expression levels in ALCL cell lines. LEMD1 was also remarkably elevated in ALCL cells (Figure 1F). ALK inhibition resulted in a potent decrease of LEMD1 and primary transcript of miR-135b (pri-miR-135b) in Karpas 299 and SUDHL-1 cells (Figure 1G), as well as in mature miR-135b, suggesting that NPM-ALK characterizes high miR-135b expression in ALCL cells. The effects of WHI-P154 on mature miR-135b were lower than those on pri-miR-135b, possibly because of generally high stability of mature miRNAs. In addition, we measured miR135b expression levels in clinical samples of ALCL patients and found that miR-135b is elevated in human primary ALK-positive ALCL samples, compared with reactive lymph node and ALK-negative ALCL samples (Figure 1H).

NPM-ALK induces LEMD1/miR-135b through STAT3 activation

To examine a direct involvement of NPM-ALK in miR-135b up-regulation in ALCL cells, we introduced wild-type and kinase-dead NPM-ALK into the human Jurkat cells and examined the expression levels of LEMD1 and miR-135b. NPM-ALK but not kinase-dead NPM-ALK (K210R) induced both LEMD1 and mature miR-135b in Jurkat cells (Figure 2A), indicating that NPM-ALK up-regulates the host gene and subsequently miR-135b through the kinase activity.

Because previous reports demonstrated that NPM-ALK elicits many downstream pathways, including STAT3, Ras-ERK, and PI3K signaling pathways,[9] we next examined the involvement of these pathways. Knockdown of NPM-ALK or STAT3 suppressed the expression of LEMD1 and miR-135b in ALCL cells (Figure 2B and supplemental Figure 1A),[12,13] whereas inhibition of ERK or PI3K failed to exert such effects (supplemental Figure 1B). We also confirmed that ca-STAT3 up-regulates LEMD1 and miR-135b in Jurkat cells (Figure 2C). Furthermore, we analyzed putative STAT3-binding sites within the conserved region of *LEMD1* gene between human and mouse and showed that STAT3 binds to putative STAT3-binding sites within the *LEMD1* genomic region by chromatin-immunoprecipitation analysis (Figure 2D-E). Reflecting high miR-135b expression, luciferase expression levels from miR-135b sensor vector were remarkably lower than those from control sensor vector in ALCL cells but not in Jurkat cells, confirming that miR-135b is highly active in ALCL cells (Figure 2F). Taken together, these results demonstrate that miR-135b lies downstream of the NPM-ALK/STAT3 signaling pathway in ALCL.

miR-135b targets FOXO1 and regulates chemosensitivity

Several potential targets of miR-135b with tumor-suppressive activities were computationally predicted previously[18] and included APC, LZTS1, LATS2, CREG1, and FOXO1. APC has been already shown as a target of miR-135b,[19] and we validated LZTS1, LATS2, and FOXO1 using luciferase reporter assay (supplemental

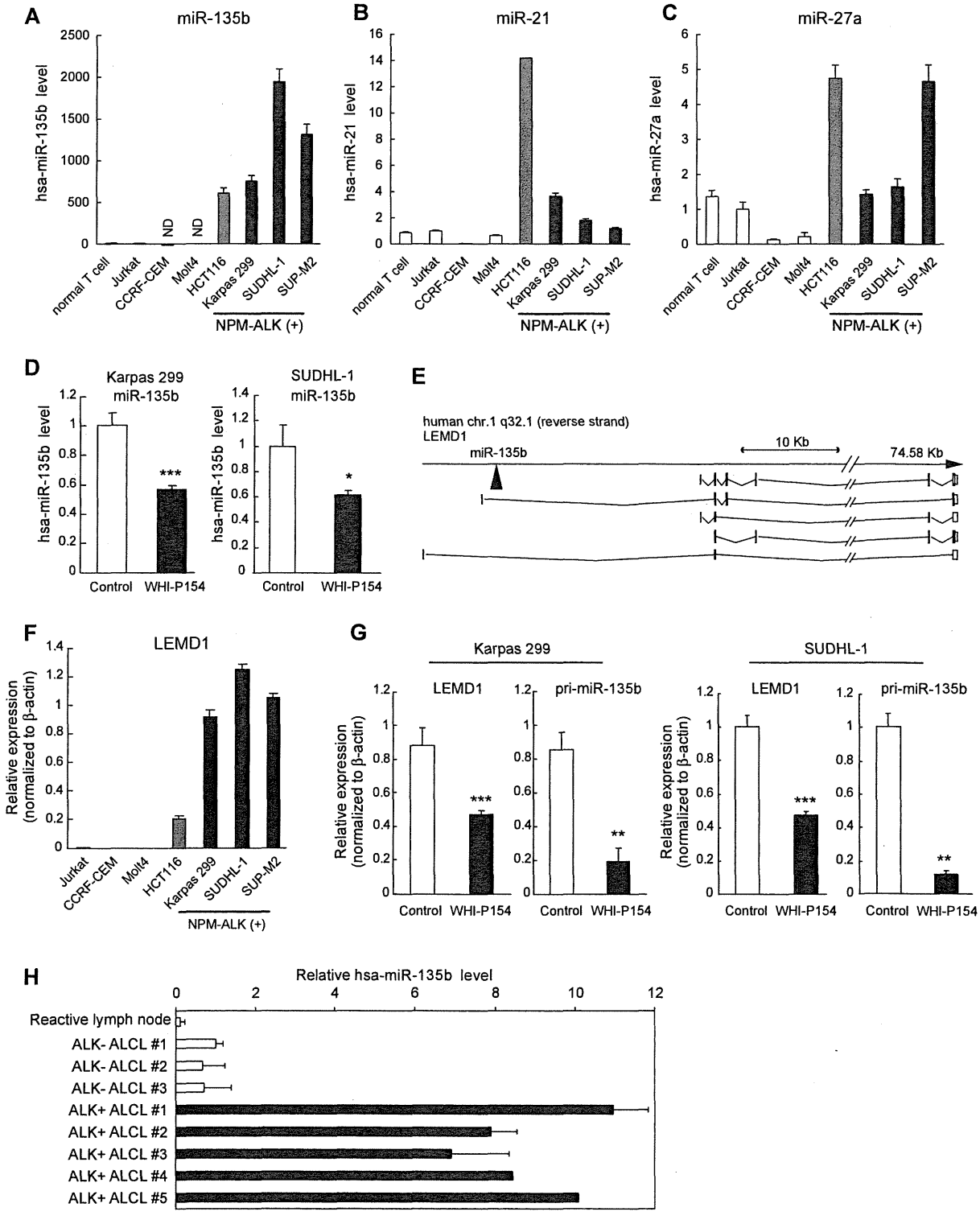

Figure 1. High expression of miR-135b and LEMD1 in ALCL. (A-C) Expression of mature miR-135b (A), miR-21 (B), and miR-27a (C) in NPM-ALK (+) ALCL cell lines (Karpas 299, SUDHL-1, and SUP-M2), normal T lymphocytes, and several T-lymphoblastic leukemia cell lines (Jurkat, CCRF-CEM, and Molt4), detected by qRT-PCR analysis. HCT116 colon cancer cells expressing endogenous miR-135b were used as positive control. ND indicates not detected. (D) Attenuation of miR-135b expression by ALK inhibitor WHI-P154. Mature miR-135b in Karpas 299 and SUDHL-1 cells was analyzed by qRT-PCR after WHI-P154 treatment (10μM, 4 hours). (E) Schematic diagram of genomic organization of human *LEMD1* gene and miR-135b. As for human *LEMD1*, several splicing variants have been reported. miR-135b is located in the first intron of *LEMD1* longer transcripts. (F) High expression of LEMD1 in ALCL cells, determined as in panel A. (G) Suppression of LEMD1 and pri-miR-135b by WHI-P154 (10μM, 1 hour) in Karpas 299 and SUDHL-1 cells, assessed as in panel D (*$P < .05$; **$P < .01$; ***$P < .001$). (H) Expression of miR-135b in clinical samples of ALCL patients.

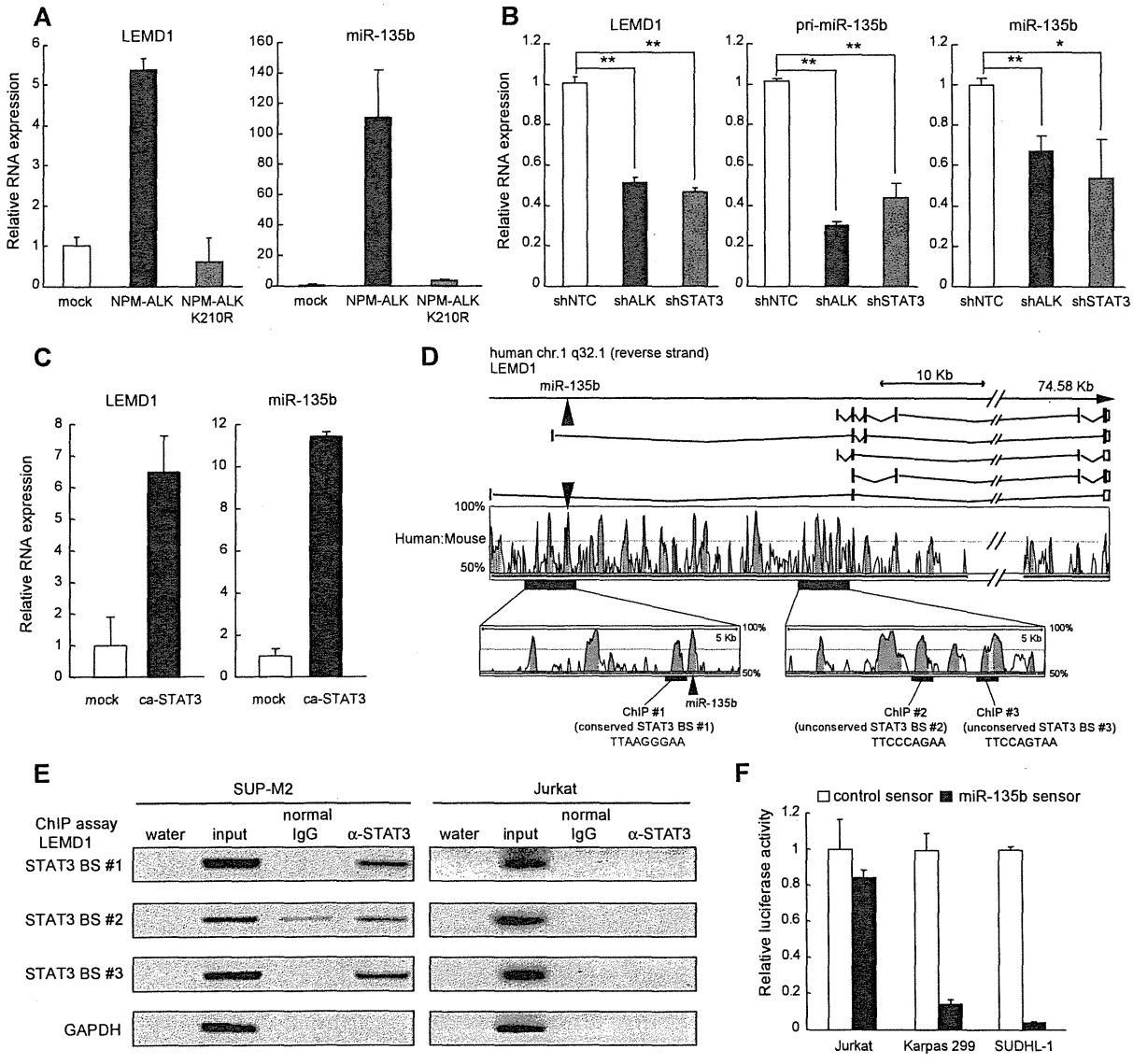

Figure 2. Identification of NPM-ALK-STAT3-miR-135b axis in ALCL. (A) Induction of LEMD1/miR-135b by NPM-ALK. Jurkat cells were transduced with lentivirus carrying NPM-ALK or kinase-dead NPM-ALK (K210R) and subjected to qRT-PCR analysis. (B) NPM-ALK/STAT3–dependent up-regulation of LEMD1/miR-135b in ALCL. Effects of shRNAs against NPM-ALK and STAT3 were evaluated in SUDHL-1 cells (*$P < .05$; **$P < .01$). (C) Up-regulation of LEMD1/miR-135b by ca-STAT3. Jurkat cells were transduced with lentivirus carrying mouse ca-STAT3 and subjected to qRT-PCR analysis. (D) STAT3 binding sites in *LEMD1* genomic region. Top panel indicates schematic genomic organization of human *LEMD1* gene and miR-135b. Sequence conservation between human and mouse is represented as the percentage of conservation in the Vista analysis shown in the middle panel. We analyzed putative STAT3-binding sites within the conserved region in ChIP analysis, and we found that STAT3 bound to 3 sites in the bottom panel, as shown in panel E. Number 1 site (TTAAGGGAA) is conserved between human and mouse. (E) Binding of STAT3 to LEMD1 genomic regions analyzed by ChIP analysis in SUP-M2 (left) and Jurkat (right) cells. Total chromatin before immunoprecipitation was used as positive control for PCR. Jurkat cells were used as negative control. (F) Enhanced miR-135b activity in ALCL. Cells were transfected with miRNA sensor vectors and applied to luciferase assay. Reflecting high miR-135b expression, luciferase expression levels from miR-135b sensor vector were remarkably lower than those from control sensor vector in ALCL cells but not in Jurkat cells.

Figure 2A-B). To identify the endogenous and functional target(s) of miR-135b in ALCL cells, we achieved the efficient long-term suppression of miR-135b activity through the decoy RNA system, in which RNA decoys against specific miRNA (TuD RNA) are driven by RNA polymerase III (Figure 3A).[11] Introduction of TuD RNA indeed strongly inhibited miR-135b activity in ALCL cell lines (Figure 3B-C and supplemental Figure 2C-D).

Using this system, we consequently identified FOXO1 as an endogenous target of miR-135b in ALCL (Figure 3D-G). The FOXO1 3′UTR contains a potential miR-135b–binding site and exogenous miR-135b suppressed FOXO1 protein expression and its translational efficiency depending on the target site, clarifying FOXO1 as a novel target of miR-135b (Figure 3D-F). Knockdown of miR-135b increased the protein expression of FOXO-dependent cell cycle inhibitors p21 and p27 as well as FOXO1 itself in ALCL cells (Figure 3G and supplemental Figure 2E). In Karpas 299 cells containing a barely detectable FOXO1, miR-135b suppression up-regulated p27 and alternatively another positive regulator of p27, CREG1 (supplemental Figure 2E).[20] Considering that NPM-ALK has been shown to inhibit FOXO3a activity through FOXO3a phosphorylation by AKT activation,[21] NPM-ALK might thus regulate a wide range of FOXO family activities via protein modification and posttranscriptional regulation. Because FOXO factors are critical mediators in growth inhibitory responses to

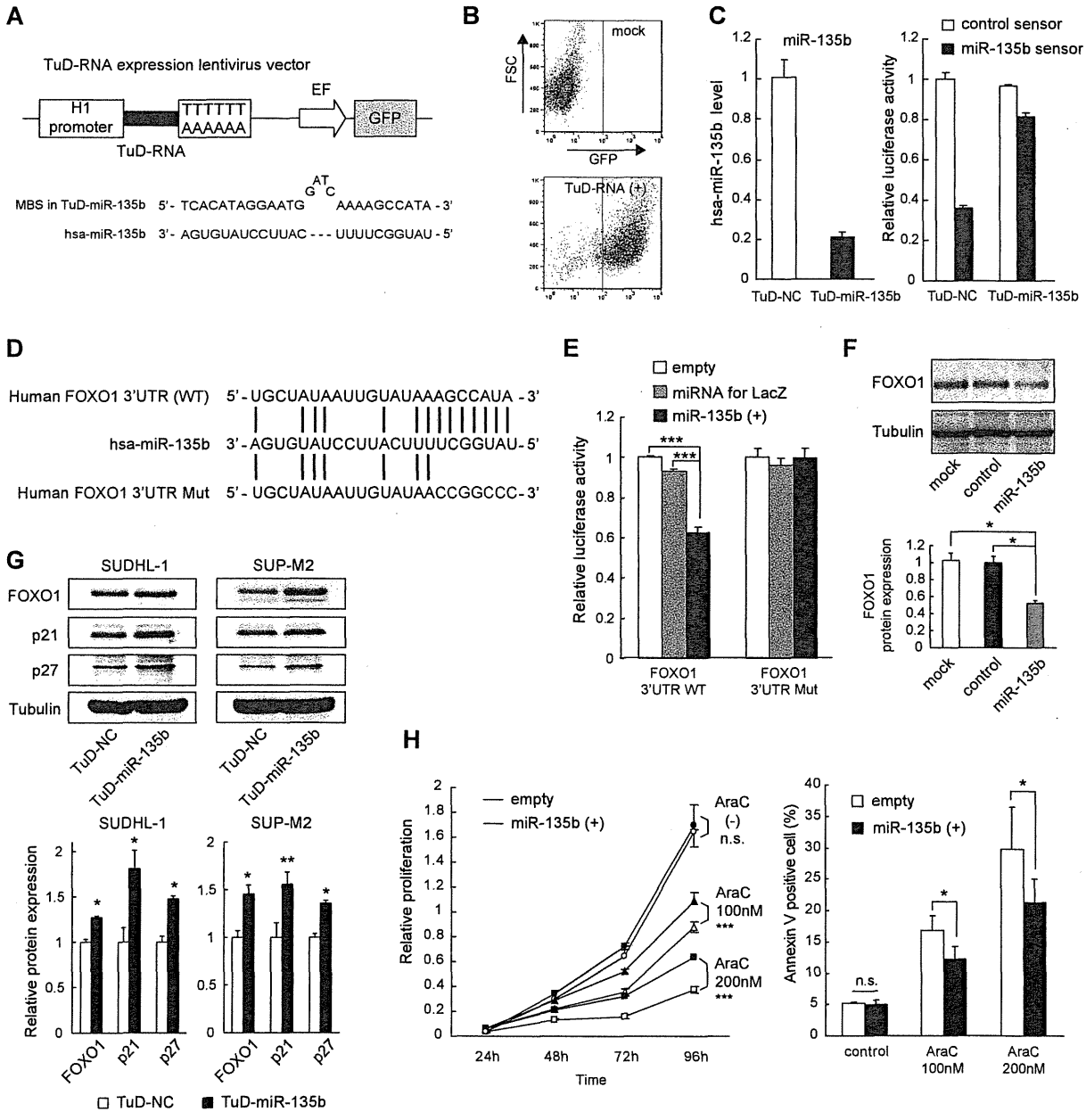

Figure 3. miR-135b targets FOXO1 and regulates chemosensitivity. (A) Structure of TuD RNA expression vector. TuD RNA for miR-135b contains miRNA-binding site (MBS) that is partially complementary to miR-135b. Details of TuD RNA structure have been described previously.[11] (B) Introduction of TuD RNA against miR-135b into ALCL cells. Flow cytometry profiles indicating transduction efficiency in Karpas 299 cells. FSC indicates forward scatter. (C) Inhibition of miR-135b function by TuD RNA for miR-135b. Left and right panels show qRT-PCR result and luciferase assay monitoring miR-135b activity, respectively. NC indicates negative control. (D) Sequence alignment between miR-135b and its putative binding site in the FOXO1 3'UTR. (E) miR-135b targets FOXO1. HEK293T cells were transfected with luciferase reporter containing the FOXO1 3'UTR with wild-type or mutated target site (shown in panel D), along with empty vector, miRNA-lacZ expression control vector (miRNA for lacZ), or pri-miR-135b expression vector [miR-135b (+)]. Luciferase assay was performed 48 hours after transfection (***$P < .001$). (F) Suppression of FOXO1 protein level by miR-135b. HeLa cells were transiently transfected with miR-135b and subjected to immunoblot analysis. (G) Elevated expression of FOXO1, p21, and p27 by miR-135b inhibition in ALCL cells. SUDHL-1 and SUP-M2 cells were infected with lentivirus harboring TuD-NC or TuD-miR-135b and applied to immunoblot analysis. The quantification results were shown in the bottom panel. (H) miR-135b–mediated attenuation of chemosensitivity. Jurkat cells with empty or pri-miR-135b vectors were treated with cytosine β-D-arabinofuranoside (AraC), followed by the assessment of cell viability (left) and apoptosis (right; *$P < .05$; ***$P < .001$; n.s., not significant).

various stresses, including DNA damage,[22] we examined the effect of miR-135b on the sensitivity to chemotherapeutic drugs to investigate functional consequences of FOXO1 alteration by miR-135b. Although miR-135 overexpression did not affect the proliferation of Jurkat cells under normal conditions, Jurkat cells overexpressing miR-135b were more resistant to cytosine β-D-arabinofuranoside (Figure 3H). These results suggest a possibility that miR-135b may confer chemoresistance to ALCL cells through FOXO1 modulation.

Targeting of Th2 regulators STAT6 and GATA3 by miR-135b

It was shown previously that constitutive activation of ALK chimeric proteins is sufficient to induce cellular transformation and

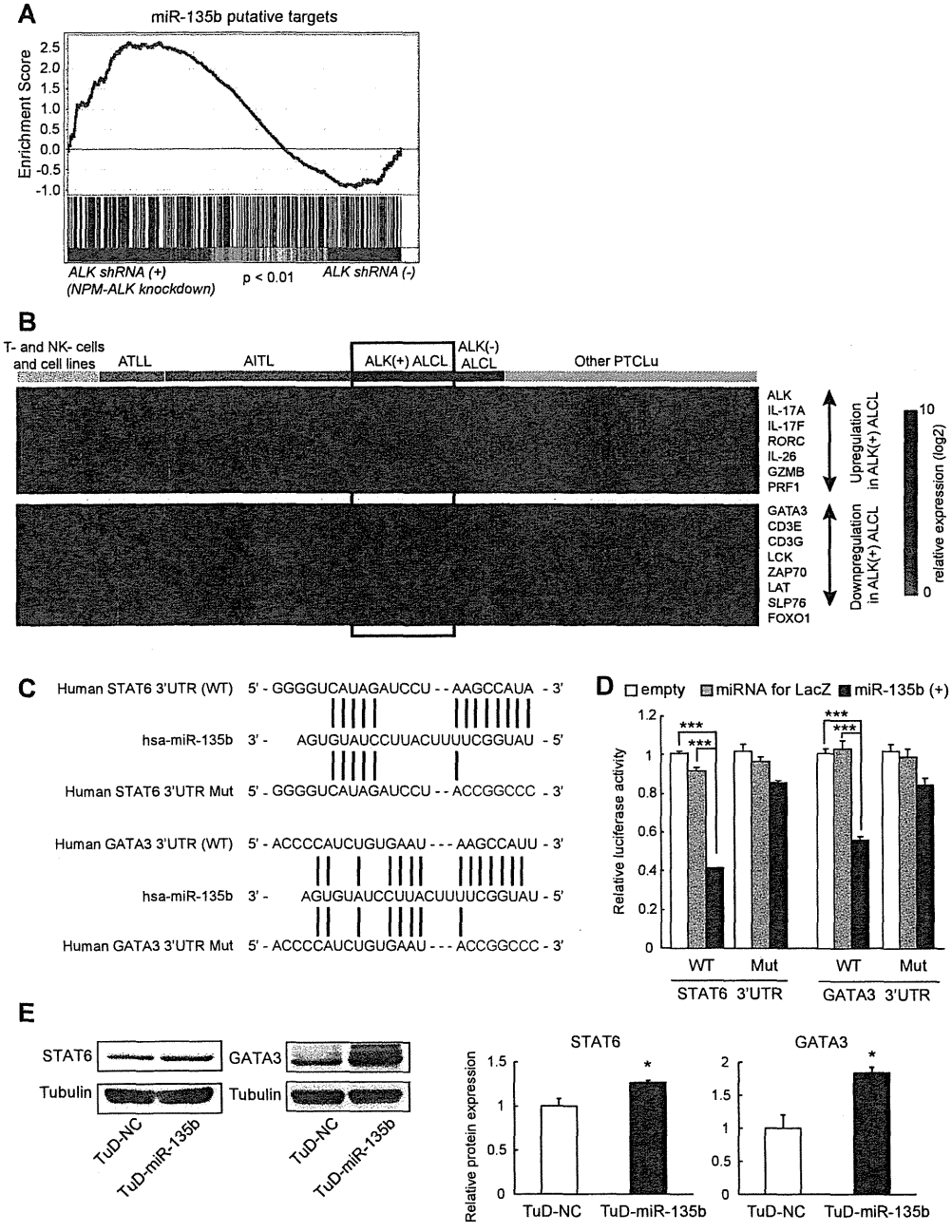

Figure 4. Targeting of STAT6 and GATA3 by miR-135b in ALCL. (A) Up-regulation of miR-135b target genes was evaluated on NPM-ALK knockdown using GSEA (dataset GSE6184). (B) Heat map showing the expression of Th17-related molecules, GATA3, FOXO1, and other ALCL-related genes (GZMB, PRF1, and TCR-related genes) in PTCL. Gene expression data are derived from GSE19069. In addition to GATA3, FOXO1 expression in ALCL was also lower than those in other PTCLs. ATLL indicates adult T-cell leukemia/lymphoma; AITL, angioimmunoblastic T-cell lymphoma; and PTCLu, PTCL-unclassifiable. (C) Sequence alignment between miR-135b and its putative binding sites in the STAT6 and GATA3 3'UTRs. (D) miR-135b targets STAT6 and GATA3. Luciferase activity of the STAT6 and GATA3 3'UTR reporter constructs with wild-type or mutated target site (shown in panel C) in HEK293T cells cotransfected with empty vector, miRNA-lacZ expression control vector (miRNA for lacZ), or pri-miR-135b expression vector [miR-135b (+)]; ***$P < .001$). (E) Up-regulation of STAT6 and GATA3 by TuD-RNA–mediated miR-135b inhibition in Karpas 299 cells. The quantification results were shown in the right panel.

that ALK activity is indispensable for the survival of ALK-positive ALCL cells.[9] In the pathogenesis of ALCL, ALK elicits reproducible transcriptome changes, as shown by previous GEP analysis.[12] To gain insight for overall interconnection between NPM-ALK–driven gene response and miR-135b–mediated gene regulation, we performed GSEA using the GEP results of ALCL cells with or without shRNA-mediated NPM-ALK inhibition.[12,16] GSEA demonstrated a significant up-regulation of miR-135b potential targets on NPM-ALK suppression, indicating that miR-135b constitutes an arm of multiple NPM-ALK downstream pathways (Figure 4A and supplemental Figure 3A). This approach suggested TGFBR1, SIRT1, cyclin G2, CREG1, Bcl11b, and STAT6 as additional candidate targets of the NPM-ALK–miR-135b pathway.

ALCL of T-lymphocyte origin has been known to present with a T- or null-cell phenotype and lack TCR complex-related molecules such as CD3ε and ZAP70, despite the presence of TCR rearrangements (Figure 4B).[23] Alternatively, recent GEP analysis in PTCL has demonstrated the following characters of ALCL cells: high

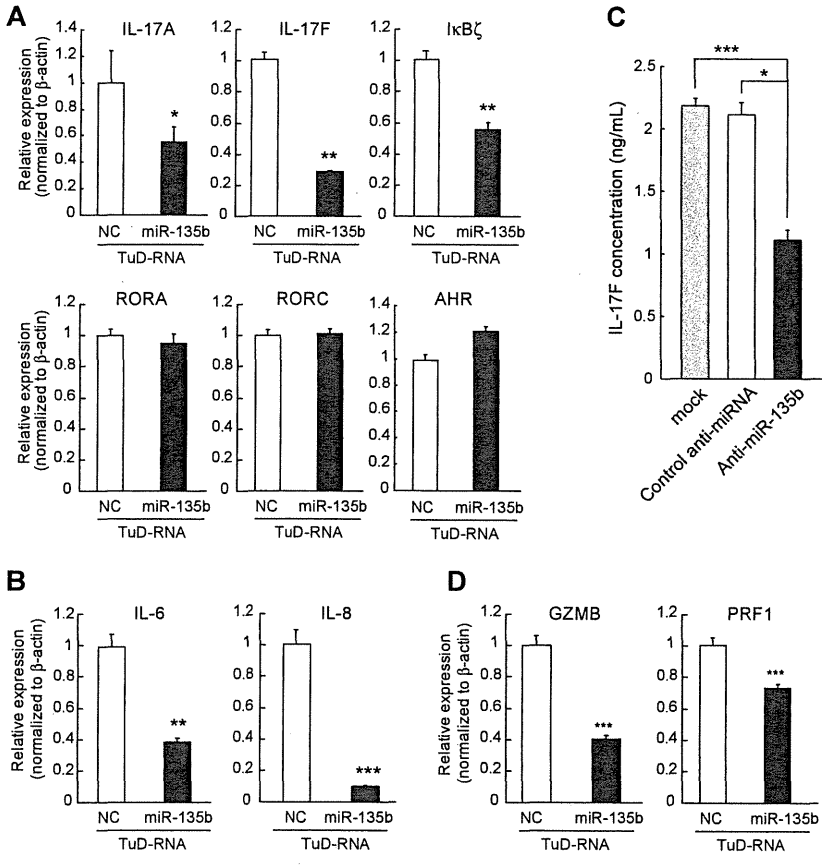

Figure 5. miR-135b blockade suppresses IL-17 production by ALCL cells and modulates ALCL immunophenotype. (A) Regulation of Th17-related molecules by miR-135b. Karpas 299 cells were infected with lentivirus harboring TuD-NC or TuD-miR-135b and applied to qRT-PCR analysis. Effects of miR-135b inhibition on the transcripts of Th17-related molecules were analyzed by qRT-PCR assay. Effects of miR-135b inhibition on IL-6 and IL-8 expression, as determined in panel A. (C) Effects of miR-135b inhibition on IL-17F production were analyzed in Karpas 299 cells by ELISA. (D) Effects of miR-135b inhibition on granzyme B (GZMB) and perforin 1 (PRF1) expression, as determined in panel A. miR-135b blockade did not affect the expression levels of IL-21, IL-23, and TGF-β1 (data not shown; $*P < .05$; $**P < .01$; $***P < .001$).

expression of Th17-cell–associated molecules (IL-17A, IL-17F, and retinoic acid-related orphan receptor [ROR]γ), overlapping with Th17 cells phenotype, low expression of GATA3, and suppression of TCR components, as summarized in Figure 4B.[15] Previous studies also have demonstrated that both Th1 and Th2 differentiation programs antagonize Th17-cell differentiation.[24]

Along with these observations, reassessment of computational prediction proposed that miR-135b potentially targets 2 Th2 master regulators GATA3 and STAT6 (Figure 4C and supplemental Figure 3B). The GSEA result also supported the possibility of STAT6 as a miR-135b target (supplemental Figure 3A). We thus investigated the immune modulatory property of miR-135b on ALCL immunophenotype overlapping with Th17 cells. Luciferase assays revealed that miR-135b targets the 3′UTRs of both STAT6 and GATA3 (Figure 4D). Mutagenesis of potential target sites in their 3′UTR abrogated the response of STAT6 and GATA3 3′UTR to miR-135b, confirming direct interactions of miR-135b with STAT6 and GATA3 (Figure 4D). We further found that suppression of miR-135b indeed up-regulates protein expression of STAT6 and GATA3 in ALCL cells, demonstrating that both STAT6 and GATA3 are intrinsic targets of miR-135b in ALCL cells (Figure 4E and supplemental Figure 3C).

miR-135b blockade suppresses IL-17 production by ALCL cells

IL-4–STAT6 axis and GATA3 are important for Th2 differentiation of normal lymphocytes.[25] In normal lymphocyte differentiation, lineage-specific transcription factors can both activate and repress differentiation programs.[26,27] GATA3 simultaneously promotes Th2 differentiation and represses Th1 differentiation, because Th1 regulator T-bet has opposing bidirectional effects.[25] A similar relationship also exists between Th1 and Th2 differentiaton programs and Th17 differentiation programs. As Th1 and Th2 effector cytokines (IFN-γ and IL-4) antagonize Th17 differentiation,[24] both GATA3 and T-bet have been shown to suppress Th17 differentiation.[27,28] On the basis of these concepts, we next examined the effects of miR-135b suppression on the expressions of Th17-related molecules. Karpas 299 ALCL cells endogenously expressed IL-17, and miR-135b suppression attenuated the expression levels of IL-17A and IL-17F transcripts (Figure 5A), consistent with GATA3-mediated suppression of Th17 differentiation.[28] Blockade of miR-135b also suppressed the expression of IκBζ, a recently identified key regulator of Th17 differentiation,[29] without concomitant changes of RORγ, RORα, or aryl hydrocarbon receptor. In addition, down-regulation of proinflammatory cytokines including IL-6 and IL-8 was observed by miR-135b suppression (Figure 5B). Consistently, we confirmed that miR-135b suppression attenuates IL-17 production in Karpas 299 cells (Figure 5C). Taken together, these findings suggest that NPM-ALK/STAT3–miR-135b axis polarizes the identity of ALCL cells to the IL-17–producing immunophenotype resembling Th17 cells by suppression of GATA3 and STAT6. In addition, miR-135b knockdown suppressed the expression of granzyme B and perforin 1, cytotoxic molecules highly expressed in ALCL (Figure 5D),[15] suggesting that miR-135b affects the broad range of ALCL immunophenotype.

Modulation of paracrine inflammatory reaction and tumorigenic potential of ALCL by miR-135b

IL-17 is a proinflammatory cytokine that stimulates the production of various inflammatory cytokines (eg, IL-1β, IL-6, IL-8, G-CSF,

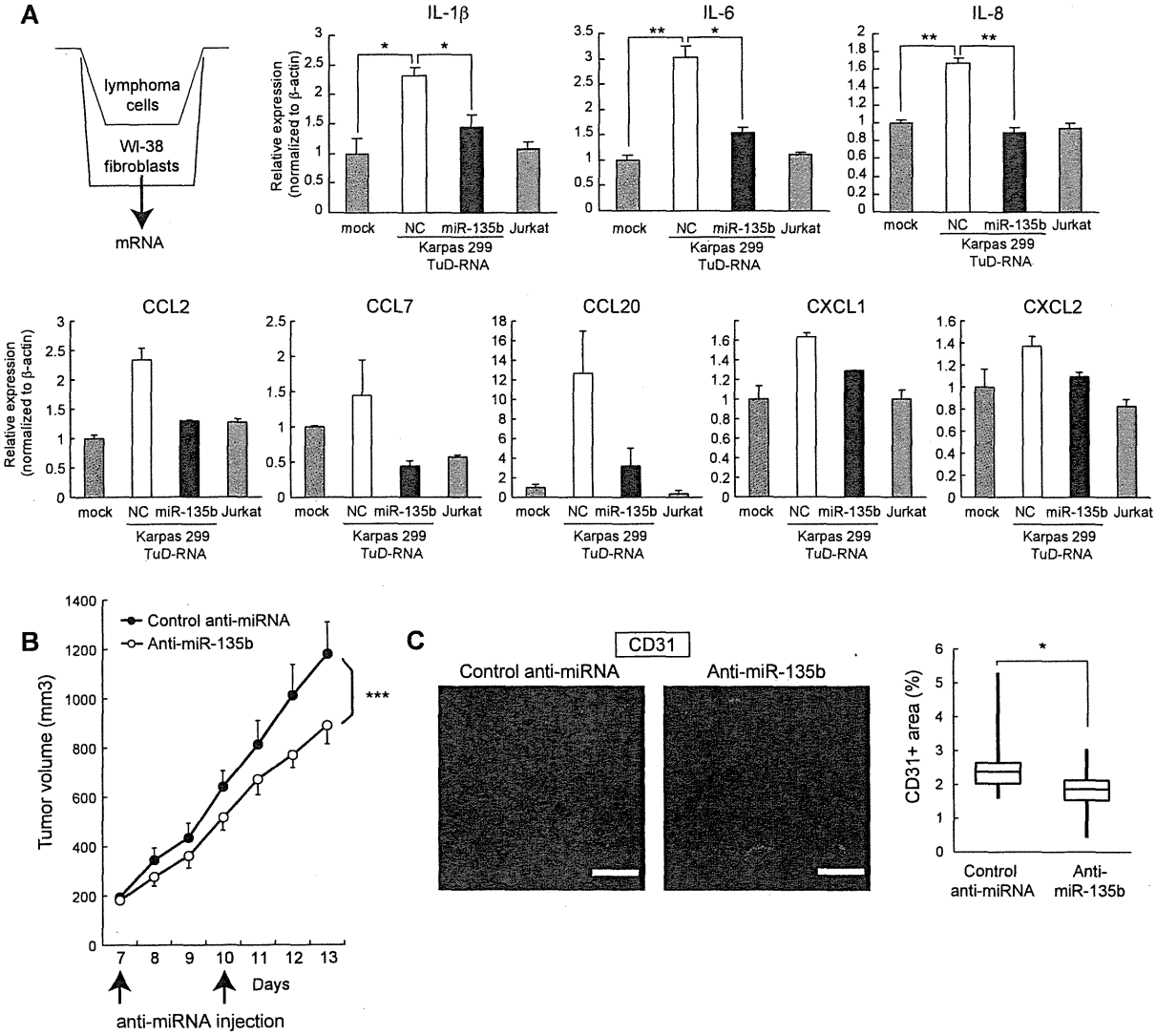

Figure 6. Regulation of paracrine inflammatory reaction and tumorigenic potential by miR-135b. (A) ALCL cells stimulate proinflammatory cytokine (IL-1β, IL-6, and IL-8) and chemokine (CCL2, CCL7, CCL20, CXCL1, and CXCL2) production in human fibroblasts through an miR-135b–dependent manner. WI-38 human fibroblasts were cocultured with Karpas 299 or Jurkat cells and subjected to qRT-PCR assay (*$P < .05$; **$P < .01$). (B) Growth curves of Karpas 299 subcutaneous tumors after transplantation into SCID mice and administration with miR-135 antisense–atelocollagen or control oligonucleotide–atelocollagen complexes. After random assignment at day 7 after inoculation (n = 6/group), LNA-based antisense oligonucleotides (5μM) with atelocollagen were administered into the subcutaneous spaces around the tumors at days 7 and 10 and measured (means ± SEM; ***$P < .001$). (C) Effects of miR-135b inhibition on tumor angiogenesis. Representative images of CD31 immunostaining of tumor sections (left) and quantification of microvessel density measured by CD31-positive area (right). Pixel density was quantified in multiple tumor images from 6 mice per group using ImageJ 1.36b software. Scale bar represents 100 μm (*$P < .05$).

and GM-CSF) and chemokines (eg, CCL2, CCL7, CCL20, CXCL1, and CXCL2) from many cell types, such as fibroblasts, endothelial cells, and neutrophils, and is involved in pathogenesis of autoimmune disorders.[30] Although the significance of IL-17 in cancer is largely unknown and might depend on cancer-type and context, proinflammatory and proangiogenic properties of IL-17 have been associated with tumor progression in several studies.[31-34] In this setting, IL-17 has been shown to augment the secretion of angiogenic chemokines, such as CXCL1 and CXCL5.[34] We analyzed the operational role of miR-135b in tumor development of ALCL. Accordingly, coculture experiments demonstrated that Karpas 299 cells stimulate the production of proinflammatory cytokines (IL-1β, IL-6, and IL-8) and chemokines (CCL2, CCL7, CCL20, and CXCL1/2) in WI-38 human fibroblasts in an miR-135b–dependent manner (Figure 6A), underscoring the involvement of miR-135b in paracrine inflammatory response.

We also examined the roles of miR-135b in ALCL tumorigenic potential in vivo. In a xenograft model, local administration of LNA-based miRNA inhibitors against miR-135b with atelocollagen suppressed the growth of subcutaneous Karpas 299 tumors (Figure 6B). Furthermore, the inhibition of in vivo tumor growth by anti–miR-135b antisense was accompanied with reduced tumor angiogenesis (Figure 6C). These results thus collectively suggest that miR-135b–mediated modulation of paracrine inflammatory reaction favors tumor microenvironment, also indicating a therapeutic significance of targeting this axis by miR-135b interference.

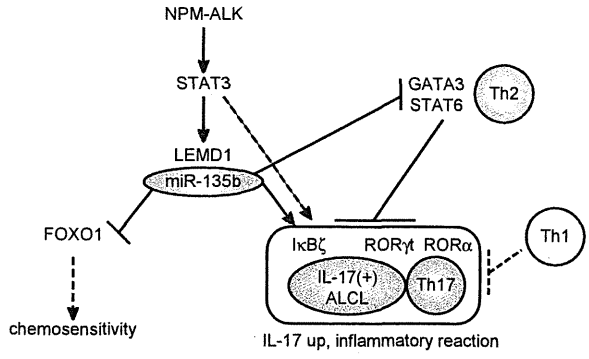

Figure 7. Summary of roles of miR-135b in ALCL pathogenesis. The present study demonstrates that NPM-ALK induces LEMD1 and miR-135b expression through STAT3 in ALCL and that miR-135b targets FOXO1 and two versatile Th2 regulators, GATA3, and STAT6, rendering the IL-17–producing immunophenotype to ALCL.

Discussion

Here, we identified miR-135b as a downstream mediator of NPM-ALK/STAT3 signaling (Figure 7). Although NPM-ALK drives malignant transformation of ALCL cells through various downstream signaling pathways, including STAT3, Ras-ERK, and PI3K,[9] our study demonstrated the oncogenic aspect of miR-135b targeting FOXO1 in ALCL pathogenesis (Figure 7). It was shown previously that miR-135b is highly expressed in embryonic stem cells and other cancer types, including colorectal and prostate cancer.[19,35,36] Considering the essential roles in embryonic stem cells and the pivotal oncogenic functions of STAT3,[37] the STAT3–miR-135b pathway might be widely used in these conditions. Oncogenic roles of miR-135b also might be supported by up-regulation of its host LEMD1, which is alternatively known as cancer/testis antigen 50, and DNA copy number gain in 1q32.1 in colorectal tumors.[38-40] Although the biologic function(s) of LEMD1 has not been investigated so far, LEMD1 also might contribute to NPM-ALK–driven oncogenicity and IL-17–producing immunophenotype in ALCL. Considering other reports linking NPM-ALK to inhibition of FOXO3a activity through PI3K/Akt pathway,[21] NPM-ALK might engage multiple players, including noncoding RNAs to prevent these central tumor suppressor pathways from activating by NPM-ALK–induced oncogenic stresses. We also examined miR-135b expression levels in lung cancer and neuroblastoma cell lines carrying ALK abnormalities (supplemental Table 4 and Figure 4). miR-135b expression was very low in neuroblastoma cell lines examined. The H2228 lung adenocarcinoma cell line containing EML4-ALK fusion expressed miR-135b to some extent, although at a lower level than ALCL cells. Involvement of miR-135b in the pathogenesis of some other tumor subtypes engaging ALK abnormalities remains to be further elucidated.

Importantly, we uncovered an interesting immune modulatory property of miR-135b. miR-135b targeted Th2 master regulators STAT6 and GATA3, and inhibition of miR-135b suppressed IL-17 production by ALCL cells, evidencing the Th17-skewing effect of miR-135b. ALK-positive ALCL is characterized by the presence of NPM-ALK and was originally described as a T- or null-cell phenotype. Loss of T-cell phenotype frequently observed in ALCL, shown by decreased expression of αβ-TCR heterodimer and CD3ε, has been demonstrated to be partly mediated by the perturbation by NPM-ALK signaling.[23] Conversely, it is postulated that the normal counterpart of ALCL is an activated mature cytotoxic T-cell, because of the expression of cytotoxic granule-associated molecules such as TIA1, gramzyme B, and perforin 1, although CD8 is usually negative in ALCL and CD4 is positive in 70% cases of ALCL.[41] In addition to this aberrant phenotype, a recent molecular signature study of PTCL revealed that ALCL displays up-regulation of Th17-cell–associated molecules (IL-17A, IL-17F, and RORγ) and down-regulation of GATA3. The immunophenotype overlaps with that of Th17 cells, compared with other lymphoma subtypes such as angioimmunoblastic T-cell lymphoma (AITL), ALK-negative ALCL, adult T-cell leukemia/lymphoma, and PTCL-unclassifiable.[15] In support of this notion, a most recent report demonstrates that levels of IL-17, IL-8, and IL-22 were elevated in untreated ALK-positive ALCL patients' sera but undetectable in those of complete remission after chemotherapy,[42] reinforcing the relevance of IL-17–producing immunophenotype of ALCL. Although the underlying mechanisms determining the immunophenotypes of various lymphomas have been largely unresolved, our study has demonstrated that a signaling network elicited by ectopic expression of NPM-ALK oncogene and its downstream miRNA confers the aberrant immunophenotype of ALCL cells.

Importance of tumor microenvironment in lymphoma development has been well investigated in B-cell lymphoma, including Hodgkin lymphoma.[43] A recent report has shown that IL-17–positive cells were more frequently observed in AITL than in PTCL-unclassifiable and that both Th17 and mast cells contribute to the lymphoma-associated proinflammatory environment in AITL.[44] In contrast, ALCL is unique in the respect that ALCL cells produce IL-17 by themselves, which might result in different clinical features between these lymphoma subtypes. In consistent with strong effects of IL-17 on neutrophils, extensive neutrophil infiltration has been observed in some cases of ALCL, as referred to as neutrophil-rich ALCL, which can sometimes be misdiagnosed as an inflammatory disease rather than lymphoma.[45-47] Frequent B symptoms in ALCL also might be attributable to this IL-17–producing immunophenotype. In this study, antisense-based miR-135b blockade reduced tumor angiogenesis and growth in an in vivo tumor model, which observation is consistent with the proangiogenic function of IL-17 (Figure 6).[33,34] Although a line of observations suggest both pro- and antitumor potentials of IL-17 or Th17 cells in a context-dependent manner,[31,32] the tumor-suppressive effect of miR-135b inhibition suggests that local proinflammatory properties of IL-17–producing ALCL cells may provide the favorable tumor microenvironment through the enhancement of angiogenesis or so in this context. Recent evidence has revealed that many characteristic aspects of cancer-related biologic processes, including drug resistance, maintenance of cancer-initiating cells, and metastasis, are associated with miRNA function.[48] The present study demonstrates another unique contribution of miRNA dysregulation to tumor development, ie, modulation of immunophenotype of lymphoma cells and the consequent alteration of tumor milieu by miR-135b.

Among hundreds of miRNAs, miR-326 has been identified so far as a regulator of Th17 differentiation, which promoted Th17 differentiation via targeting ETS1.[49] In addition, miR-155 was recently shown to promote Th17 cell formation in a $CD4^+$ T-cell intrinsic manner.[50] It was consistent with the finding that miR-155 targets Th2 promoter c-Maf. Our study suggests the presence of additional regulatory miRNAs of Th17 differentiation through the inhibition of differentiation program(s) to other helper T-cell lineage(s). Generally, lineage-specific transcription factors and cytokines can interfere with the differentiation to other helper T-cell subsets. Although it requires careful assessment about

difference between normal lymphocyte differentiation and lymphoma cell phenotype polarization, our findings suggest that miRNAs might be widely involved in this reciprocal regulatory network between helper T-cell differentiation programs. The STAT3–miR-135b–GATA3/STAT6 connection revealed in this study might propose inhibitory mechanism(s) against Th2 in Th17 differentiation program, mirroring the opposite inhibitory impacts of Th1 and Th2 programs on Th17 differentiation,[24,26] for ensuring mutual exclusion.

In conclusion, our study demonstrates a novel oncogenic pathway composed of NPM-ALK, STAT3, and miR-135b that authorizes IL-17–producing immunophenotype of ALCL. Tumor suppression with miR-135b blockade also demonstrates the therapeutic potential of miR-135b interference strategy targeting the "Th17 mimic" axis. These findings might advance our understandings of ALK-mediated oncogenesis and be useful for the development of new therapeutic interventions.

Acknowledgments

The authors thank E. Johansson, Y. Morishita, K. Kiyono, M. Morikawa, Y. Yoshimatsu, K. Isogaya, and H. Mihira for discussion and skilled technical assistance and all members of the Department of Molecular Pathology, University of Tokyo.

This work was supported by KAKENHI (Grants-in-Aid for Scientific Research for Research Activity start-up 22890038 and Innovative Areas "RNA regulation" 23112702); the Global Center of Excellence Program for "Integrative Life Science Based on the Study of Biosignaling Mechanisms" from the Ministry of Education, Culture, Sports, Science and Technology of Japan; and the Cell Science Research Foundation.

Authorship

Contribution: H. Matsuyama and H.I.S. conceived and designed the research; H. Matsuyama performed experiments and analyses and wrote the paper; H.I.S. provided key materials and analyzed and wrote the paper; H.N. performed animal experiments and analysis; M.N., T.Y., N.K., H. Mano and K.S. provided clinical samples; and K.S. and K.M. supervised the whole project and wrote the paper.

Conflict-of-interest disclosure: The authors declare no competing financial interests.

Correspondence: Kohei Miyazono, Department of Molecular Pathology, Graduate School of Medicine, University of Tokyo, 7-3-1 Hongo, Bunkyo-ku, Tokyo 113-0033, Japan; e-mail: miyazono@m.u-tokyo.ac.jp.

References

1. Ambros V, Chen X. The regulation of genes and genomes by small RNAs. *Development.* 2007; 134(9):1635-1641.
2. O'Connell RM, Rao DS, Chaudhuri AA, Baltimore D. Physiological and pathological roles for microRNAs in the immune system. *Nat Rev Immunol.* 2010; 10(2):111-122.
3. Croce CM. Causes and consequences of microRNA dysregulation in cancer. *Nat Rev Genet.* 2009;10(10):704-714.
4. Staudt LM, Dave S. The biology of human lymphoid malignancies revealed by gene expression profiling. *Adv Immunol.* 2005;87:163-208.
5. Alizadeh AA, Eisen MB, Davis RE, et al. Distinct types of diffuse large B-cell lymphoma identified by gene expression profiling. *Nature.* 2000; 403(6769):503-511.
6. Suzuki HI, Miyazono K. Emerging complexity of microRNA generation cascades. *J Biochem.* 2011;149(1):15-25.
7. He L, Thomson JM, Hemann MT, et al. A microRNA polycistron as a potential human oncogene. *Nature.* 2005;435(7043):828-833.
8. Suzuki HI, Yamagata K, Sugimoto K, Iwamoto T, Kato S, Miyazono K. Modulation of microRNA processing by p53. *Nature.* 2009;460(7254):529-533.
9. Chiarle R, Voena C, Ambrogio C, Piva R, Inghirami G. The anaplastic lymphoma kinase in the pathogenesis of cancer. *Nat Rev Cancer.* 2008;8(1):11-23.
10. Soda M, Choi YL, Enomoto M, et al. Identification of the transforming EML4-ALK fusion gene in non-small-cell lung cancer. *Nature.* 2007; 448(7153):561-566.
11. Haraguchi T, Ozaki Y, Iba H. Vectors expressing efficient RNA decoys achieve the long-term suppression of specific microRNA activity in mammalian cells. *Nucleic Acids Res.* 2009;37(6):e43.
12. Piva R, Pellegrino E, Mattioli M, et al. Functional validation of the anaplastic lymphoma kinase signature identifies CEBPB and BCL2A1 as critical target genes. *J Clin Invest.* 2006;116(12):3171-3182.
13. Anastasov N, Klier M, Koch I, et al. Efficient shRNA delivery into B and T lymphoma cells using lentiviral vector-mediated transfer. *J Hematop.* 2009;2(1):9-19.
14. Bromberg JF, Wrzeszczynska MH, Devgan G, et al. Stat3 as an oncogene. *Cell.* 1999;98(3): 295-303.
15. Iqbal J, Weisenburger DD, Greiner TC, et al. Molecular signatures to improve diagnosis in peripheral T-cell lymphoma and prognostication in angioimmunoblastic T-cell lymphoma. *Blood.* 2010; 115(5):1026-1036.
16. Subramanian A, Tamayo P, Mootha VK, et al. Gene set enrichment analysis: a knowledge-based approach for interpreting genome-wide expression profiles. *Proc Natl Acad Sci U S A.* 2005;102(43):15545-15550.
17. Lawrie CH, Saunders NJ, Soneji S, et al. MicroRNA expression in lymphocyte development and malignancy. *Leukemia.* 2008;22(7): 1440-1446.
18. Saito T, Saetrom P. MicroRNAs–targeting and target prediction. *N Biotechnol.* 2010; 27(3):243-249.
19. Nagel R, le Sage C, Diosdado B, et al. Regulation of the adenomatous polyposis coli gene by the miR-135 family in colorectal cancer. *Cancer Res.* 2008;68(14):5795-5802.
20. Kuiper RP, Schoenmakers EF, van Reijmersdal SV, et al. High-resolution genomic profiling of childhood ALL reveals novel recurrent genetic lesions affecting pathways involved in lymphocyte differentiation and cell cycle progression. *Leukemia.* 2007;21(6):1258-1266.
21. Gu TL, Tothova Z, Scheijen B, Griffin JD, Gilliland DG, Sternberg DW. NPM-ALK fusion kinase of anaplastic large-cell lymphoma regulates survival and proliferative signaling through modulation of FOXO3a. *Blood.* 2004;103(12): 4622-4629.
22. Greer EL, Brunet A. FOXO transcription factors at the interface between longevity and tumor suppression. *Oncogene.* 2005;24(50):7410-7425.
23. Ambrogio C, Martinengo C, Voena C, et al. NPM-ALK oncogenic tyrosine kinase controls T-cell identity by transcriptional regulation and epigenetic silencing in lymphoma cells. *Cancer Res.* 2009;69(22):8611-8619.
24. Harrington LE, Hatton RD, Mangan PR, et al. Interleukin 17-producing CD4+ effector T cells develop via a lineage distinct from the T helper type 1 and 2 lineages. *Nat Immunol.* 2005;6(11):1123-1132.
25. Zhou M, Ouyang W. The function role of GATA-3 in Th1 and Th2 differentiation. *Immunol Res.* 2003;28(1):25-37.
26. McGeachy MJ, Cua DJ. Th17 cell differentiation: the long and winding road. *Immunity.* 2008;28(4): 445-453.
27. Lazarevic V, Chen X, Shim JH, et al. T-bet represses T(H)17 differentiation by preventing Runx1-mediated activation of the gene encoding RORgammat. *Nat Immunol.* 2011;12(1):96-104.
28. van Hamburg JP, Mus AM, de Bruijn MJ, et al. GATA-3 protects against severe joint inflammation and bone erosion and reduces differentiation of Th17 cells during experimental arthritis. *Arthritis Rheum.* 2009;60(3):750-759.
29. Okamoto K, Iwai Y, Oh-Hora M, et al. Ikappa-Bzeta regulates T(H)17 development by cooperating with ROR nuclear receptors. *Nature.* 2010; 464(7293):1381-1385.
30. Yang XO, Chang SH, Park H, et al. Regulation of inflammatory responses by IL-17F. *J Exp Med.* 2008;205(5):1063-1075.
31. Ji Y, Zhang W. Th17 cells: positive or negative role in tumor? *Cancer Immunol Immunother.* 2010;59(7):979-987.
32. Zou W, Restifo NP. T(H)17 cells in tumour immunity and immunotherapy. *Nat Rev Immunol.* 2010; 10(4):248-256.
33. Numasaki M, Fukushi J, Ono M, et al. Interleukin-17 promotes angiogenesis and tumor growth. *Blood.* 2003;101(7):2620-2627.
34. Numasaki M, Watanabe M, Suzuki T, et al. IL-17 enhances the net angiogenic activity and in vivo growth of human non-small cell lung cancer in SCID mice through promoting CXCR-2-dependent angiogenesis. *J Immunol.* 2005;175(9): 6177-6189.

35. Lin CH, Jackson AL, Guo J, Linsley PS, Eisenman RN. Myc-regulated microRNAs attenuate embryonic stem cell differentiation. *EMBO J.* 2009;28(20):3157-3170.
36. Tong AW, Fulgham P, Jay C, et al. MicroRNA profile analysis of human prostate cancers. *Cancer Gene Ther.* 2009;16(3):206-216.
37. Bowman T, Garcia R, Turkson J, Jove R. STATs in oncogenesis. *Oncogene.* 2000;19(21):2474-2488.
38. Yuki D, Lin YM, Fujii Y, Nakamura Y, Furukawa Y. Isolation of LEM domain-containing 1, a novel testis-specific gene expressed in colorectal cancers. *Oncol Rep.* 2004;12(2):275-280.
39. Jones AM, Douglas EJ, Halford SE, et al. Array-CGH analysis of microsatellite-stable, near-diploid bowel cancers and comparison with other types of colorectal carcinoma. *Oncogene.* 2005; 24(1):118-129.
40. Douglas EJ, Fiegler H, Rowan A, et al. Array comparative genomic hybridization analysis of colorectal cancer cell lines and primary carcinomas. *Cancer Res.* 2004;64(14):4817-4825.
41. Swerdlow SH, Campo E, Harris NL, et al. *WHO Classification of Tumours of Haematopoietic and Lymphoid Tissues.* 4th ed. Lyon, France: IARC; 2008.
42. Savan R, McFarland AP, Reynolds DA, et al. A novel role for IL-22R1 as a driver of inflammation. *Blood.* 2011;117(2):575-584.
43. Küppers R. The biology of Hodgkin's lymphoma. *Nat Rev Cancer.* 2009;9(1):15-27.
44. Tripodo C, Gri G, Piccaluga PP, et al. Mast cells and Th17 cells contribute to the lymphoma-associated pro-inflammatory microenvironment of angioimmunoblastic T-cell lymphoma. *Am J Pathol.* 2010;177(2):792-802.
45. Mann KP, Hall B, Kamino H, Borowitz MJ, Ratech H. Neutrophil-rich, Ki-1-positive anaplastic large-cell malignant lymphoma. *Am J Surg Pathol.* 1995;19(4):407-416.
46. Tamiolakis D, Georgiou G, Prassopoulos P, Simopoulos C, Venizelos J, Papadopoulos N. Neutrophil-rich anaplastic large cell lymphoma (NR-ALCL) mimicking lymphadenitis: a study by fine-needle aspiration biopsy. *Leuk Lymphoma.* 2004; 45(6):1309-1310.
47. Engsig FN, Moller MB, Hasselbalch HK, Mahdi B, Obel N. Extreme neutrophil granulocytosis in a patient with anaplastic large cell lymphoma of T-cell lineage. *APMIS.* 2007;115(6):778-783.
48. Suzuki HI, Miyazono K. Dynamics of microRNA biogenesis: crosstalk between p53 network and microRNA processing pathway. *J Mol Med.* 2010; 88(11):1085-1094.
49. Du C, Liu C, Kang J, et al. MicroRNA miR-326 regulates TH-17 differentiation and is associated with the pathogenesis of multiple sclerosis. *Nat Immunol.* 2009;10(12):1252-1259.
50. O'Connell RM, Kahn D, Gibson WS, et al. MicroRNA-155 promotes autoimmune inflammation by enhancing inflammatory T cell development. *Immunity.* 2010;33(4):607-619.

Dicer Plays Essential Roles for Retinal Development by Regulation of Survival and Differentiation

Atsumi Iida,[1,2] *Toru Shinoe,*[1,2] *Yukihiro Baba,*[1] *Hiroyuki Mano,*[3] *and Sumiko Watanabe*[1]

Purpose. Much attention has been paid to the roles of microRNA in developmental and biological processes. Dicer plays essential roles in cell survival and proliferation in various organs. We examined the role of Dicer in retinal development using retina-specific conditional knockout of Dicer in mice.

Methods. Dkk3-Cre expressed the *Cre* gene in retinal progenitor cells from an early embryonic stage. The authors analyzed Dkk-Cre/Dicer-flox (Dicer-CKO) mice for their survival, proliferation, and differentiation. To analyze the role of Dicer in later stages of retinal development, a Cre expression plasmid was introduced into the neonatal retina by electroporation, and retinal differentiation was examined.

Results. Dicer-CKO mice were born at the numbers we expected, based on Mendelian genetics, but their eyes never opened. Massive death of retinal progenitor cells occurred during embryogenesis, resulting in microphthalmia, and most retinal cells had disappeared by postnatal day 14. In vitro reaggregation culture of Dicer-CKO retinal cells showed that cell death and the suppression of proliferation by Dicer inactivation occurred in a cell-autonomous manner. Cell differentiation markers were expressed in the Dicer-CKO retina; however, these cells localized abnormally, and the inner plexiform layer was absent, suggesting that cell migration and morphologic differentiation, especially process extension, were perturbed. Forced neonatal expression of Cre induced apoptosis and affected the expression of differentiation markers.

Conclusions. Taken together, these results show that Dicer is essential during early retinal development. (*Invest Ophthalmol Vis Sci.* 2011;52:3008-3017) DOI:10.1167/iovs.10-6428

The vertebrate neural retina is organized into a laminar structure comprising six types of neuron and glial cell, including Müller glia and microglia. During retinogenesis, these various cell types are derived from a common population of multipotent retinal progenitor cells in a relatively fixed chronological sequence.[1] Intrinsic cues and extrinsic signals play critical roles in defining the types of cells generated from common retinal progenitor cells,[2,3] and various molecules are involved in this process. The expression of these genes in retinal development is regulated at various levels; microRNA (miRNA) is one such regulator.

MicroRNAs are small, noncoding RNAs that are encoded in the genomes of all metazoans. They are essential in the proliferation and differentiation of various tissues, including stem cells.[4-6] The roles of miRNAs in retina have been reported,[7,8] and a recent study showed the presence of light-regulated retinal miRNAs.[9] In addition to suppressing the function of certain miRNAs, we can remove all miRNAs by deleting enzymes that are essential in their biosynthesis. DGCR8 is required for the production of all canonical miRNAs, and Dicer is an enzyme that cleaves double-stranded RNA into miRNA.[10] The removal of DGCR8 or Dicer results in a defective cell cycle and silencing of the self-renewal program of embryonic stem cells.[11,12] Because the complete loss of Dicer in mice results in early embryonic death,[13] mice with a conditional allele of the Dicer gene have been produced,[14] enabling the study of the roles of miRNA in organogenesis. Subsequently, essential roles of Dicer in organogenesis have been revealed by studying mice with various tissue-specific expression of Cre.[14,15]

In neurons, the deletion of Dicer by α-calmodulin kinase II Cre results in an array of phenotypes, including microcephaly and reduced dendritic branch elaboration, suggesting that the loss of Dicer disrupts cellular and tissue morphogenesis in the cortex and hippocampus.[16] The first study examining the roles of Dicer in the retina using Chx10-Cre transgenes, expected to express Cre in retinal progenitor cells, showed that although Chx10 was expressed in the embryonic retina, morphologic defects were observed at postnatal day (P) 16 with the formation of photoreceptor rosettes, accompanied by abnormal electroretinogram responses.[17] However, the relatively mild phenotype of the mice is surmised to be caused by mosaic expression of Cre in the Chx10-Cre transgenic retina[17] because subsequent work by George and Reh using αPax6-Cre-retina specific Dicer conditional knockout showed that Dicer is required in retinal development.[18] In this work, we evaluated the effects of deleting Dicer using Dkk3-Cre mice, which expressed the *Cre* gene in retinal progenitor cells from an early embryonic stage.[19]

Materials and Methods

Mice and Reagents

EGFP transgenic mice, which express the *EGFP* gene ubiquitously through the CAG promoter, were kindly provided by Masaru Okabe (Osaka University).[20,21] $Dicer^{flox}$ mice[14] were kindly provided by Michael McManus (University of California, San Francisco), and Dkk3-Cre BAC transgenic mice were as previously described.[19] $Dicer^{flox/flox}$ (Dicer-fl/fl) or $Dicer^{flox/wild}$ were used as controls for experiments shown in Figures 1 and 2. ICR mice were obtained from Japan SLC Co. All animal experiments were approved by the Animal Care Committee of the Institute of Medical Science, University of Tokyo, and were conducted in accordance with the ARVO Statement for the Use of Animals in Ophthalmic and Vision Research.

From the [1]Division of Molecular and Developmental Biology, Institute of Medical Science, University of Tokyo, Tokyo, Japan; and the [3]Division of Functional Genomics, Jichi Medical University, Tochigi, Japan.

[2]These authors contributed equally to the work presented here and should therefore be regarded as equivalent authors.

Supported by MEXT, Japan.

Submitted for publication August 18, 2010; revised October 18 and December 7 and 14, 2010; accepted December 15, 2010.

Disclosure: **A. Iida**, None; **T. Shinoe**, None; **Y. Baba**, None; **H. Mano**, None; **S. Watanabe**, None

Corresponding author: Sumiko Watanabe, Division of Molecular and Developmental Biology, Institute of Medical Science, University of Tokyo, 4-6-1 Shirokanedai, Minato-ku, Tokyo 108-8639, Japan; sumiko@ims.u-tokyo.ac.jp.

Investigative Ophthalmology & Visual Science, May 2011, Vol. 52, No. 6

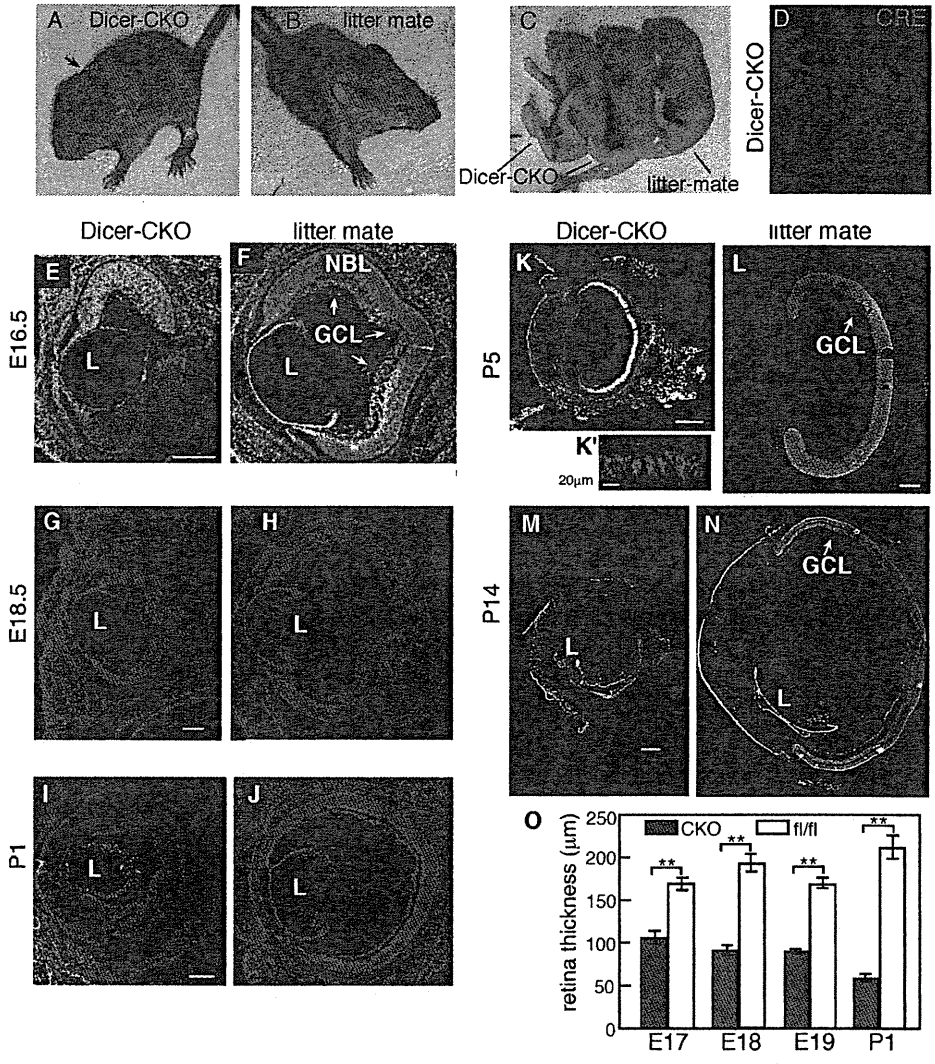

FIGURE 1. Dicer$^{lox/lox}$:Dkk3$^{+/cre}$ (Dicer-CKO) mice were born but had microphthalmia. (**A–C**) Images of Dicer-CKO (**A**) and littermate (**B**) mice at 2 weeks of age. Images of embryos of Dicer-CKO and littermate at E16.5 (**C**). (**D**) Immunostaining of Cre expression of Dicer-CKO retina at E17.5 was performed using frozen sections. (**E–N**) Structure of the eye of Dicer-CKO and littermate at E16.5 (**E**, **F**), E18.5 (**G**, **H**), P1 (**I**, **J**), P5 (**K**, **L**), and P14 (**M**, **N**) stages. Head (**E–J**) or whole eyes (**K–N**) were frozen sectioned, and nuclei were visualized by staining of DAPI. L, lens. Scale bar, 200 μm unless indicated. L, lens; NBL, neuroblastic layer. (**O**) Thickness of retina of Dicer-CKO or fl/fl control mice. Measurements were made under a microscope, and the thickness of retina at central region was examined at indicated stages. Average of three independent retinas with SD is shown. $^{**}P < 0.01$, Student's *t*-test.

DNA Construction

pxCANCre containing CAG promoter followed by *Cre* genes was the gift of Izumu Saito (University of Tokyo). CAG-Cre-IRES-EGFP was constructed by the ligation of fragments of CAG-Cre (*SalI-BglII*), IRES-EGFP (*BglII-NotI*), and the vector portion from pEGFP2 (*SalI-NotI*).

Immunostaining

Immunostaining of sectioned or dissociated retina was performed as described previously.[22] OCT compound (Tissue-Tek)–embedded samples were sectioned with 10-μm thickness by a cryostat (CM3050S; Leica, Wetzlar, Germany). Primary antibodies used were the following: mouse monoclonal antibodies against βIII tubulin (Covance, Princeton, NJ), photoreceptor-specific nuclear receptor ([PNR], ppmx), rhodopsin (Rho4D2, kindly donated by Robert S. Molday, University of British Columbia), glutamine synthetase (GS; Chemicon, Temecula, CA), HuC/D (Molecular Probes, Eugene, OR), Ki67 (BD Biosciences, Franklin Lakes, NJ), Cre (Millipore, Billerica, MA), rabbit polyclonal antibody against GFP (Clontech, Palo Alto, CA), Pax6 (Covance), calbindin (Millipore), active-caspase3 (Promega, Madison, WI), and goat polyclonal antibody anti-Brn3b (Santa Cruz Biotechnology, Santa Cruz, CA). All antibodies against retinal subtypes have been used by us and confirmed to recognize mouse retina.[23–25] The first antibodies were visualized by using appropriate Alexa 488 or Alexa 546-conjugated secondary antibodies (Molecular Probes). Samples were mounted in reagent (VectaShield; Vector Laboratories, Burlingame, CA) and analyzed under a microscope (Axioplan; Zeiss, Oberkochen, Germany).

Retinal Cultures and Electroporation

Reaggregation cultures were set up as described earlier.[23] Briefly, retinal cells of Dicer-CKO:GFP or GFP mice at embryonic day (E) 16 were dissociated and mixed with far larger numbers of host retinal cells isolated from normal ICR mice at E16. The ratio of donor to host cells was 5:95. Electroporation was performed using an electroporator (CUY21; Nepa Gene, Chiba, Japan) and electrode (CYU520P5; Nepa Gene), as described.[26] Briefly, retinas were transferred to a microelectroporation chamber filled with plasmid solution (1 mg/mL in Hanks' balanced salt solution), and four square pulses (25 V) of 50-μs duration with 950-μs intervals were applied using a pulse generator (CUY21; Nepa Gene).

RESULTS

Inactivation of Dicer in Retinal Progenitor Cells Results in Severe Retinal Malformation

To inactivate Dicer in retinal progenitor cells, we used Dkk3-Cre mice, which express Cre recombinase beginning on at least E10.5 in a retina-specific manner.[19] The expected num-

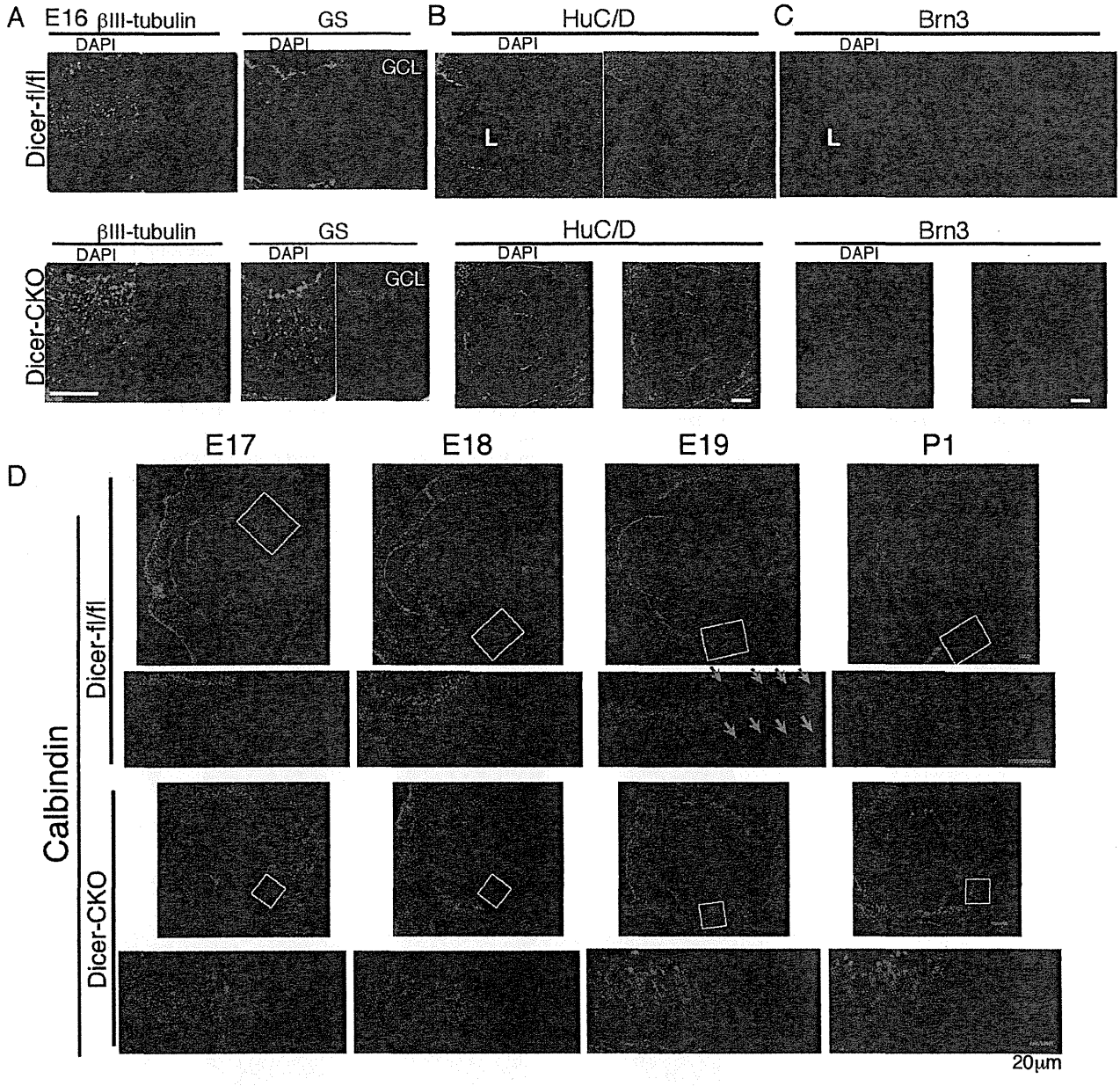

FIGURE 2. Detailed examination of retinal development by immunostaining of retinas of Dicer-CKO mice revealed perturbation of retinal development. (**A–D**) Retinas from Dicer-CKO or littermate control mice at E16 (**A–C**) or indicated stages (**D**) were frozen sectioned. Immunostaining using indicated antibodies was performed, and nuclei were visualized by staining of DAPI. (**D**) *Lower* panels are enlarged images of the *white squared regions* in the *upper* panels. L, lens. Scale bars: 100 μm (**A**, **D**); 200 μm (**B**, **C**).

bers of $Dicer^{flox/flox}/Dkk3^{cre/-}$ (Dicer-CKO) mice, based on Mendelian genetics, were born, but they died approximately 4 to 6 weeks after birth for unknown reasons. Their eyes never opened (Fig. 1A), and they had small earlobes (Fig. 1A, red arrows), probably because of undetectable expression of Dkk3 in this region. The Dicer-CKO embryos were indistinguishable from their littermates in their appearance, except for their small eyes (Fig. 1C). During development, we examined eye structure in more detail using frozen sections. We first confirmed that Cre was expressed in nearly the whole area of the retina at E17.5 (Fig. 1D), as expected from the expression pattern of Dkk3-Cre original mice.[19] At E16.5, the retinas of the Dicer-CKO mice were already smaller than those of control mice (Figs. 1E, 1F). At this stage, the ganglion cell layer (GCL) was visible in control (Fig. 1E, arrows) but not in the Dicer-CKO (Fig. 1E) mice. At E18.5, the difference between retinal sphere diameters in the Dicer-CKO and littermates became clearer (Figs. 1G, 1H). At P1, the GCL and the inner plexiform layer (IPL) were clearly formed in the control retinas (Fig. 1J) but had not formed in the Dicer-CKO retinas. Retinal diameters were even smaller than those at E16.5 in Dicer-CKO mice, and the cells were not tightly linked (Fig. 1I). At P5, the retina was very thin, and no layered structure was observed in the Dicer-CKO mice (Fig. 1K'). At P14, the retina had no visible structure in Dicer-CKO mice, and there only a few cell aggregates remained in the central region in Dicer-CKO retinas (Fig. 1M).

We measured retinal thickness. Retinas of Dicer-CKO were thinner than those of control mice at E17 and constantly became thinner as development proceeded (Fig. 1O).

Differentiation Markers of Retinal Subtypes Were Once Expressed, Then Disappeared, as Retinal Development Proceeded

To examine the differentiation of retinal subtypes in the Dicer-CKO retina, we immunostained various markers of retinal subtypes using frozen sections. At first, control staining to examine nonspecific signal was performed using frozen, sectioned retinas at E17 and P6. Control immunoglobulin was used as the first antibody, and appropriate second antibodies conjugated with either Alexa 488 or Alexa 594 were stained. With E17 samples, mouse IgG showed nonspecific staining in regions around the GCL and inner nuclear layer (INL), which was thought to be the blood vessel, and rat primary antibody gave no significant nonspecific staining (Supplementary Fig. S1, http://www.iovs.org/lookup/suppl/doi:10.1167/iovs.10-6428/-/DCSupplemental). At P6, signals around GCL in mouse IgG antibodies, but not in the rat IgG antibody, were observed (Supplementary Fig. S1, http://www.iovs.org/lookup/suppl/doi:10.1167/iovs.10-6428/-/DCSupplemental). At E16, although the control retina had no layer structure except for the GCL, the inner half of the cells had became postmitotic whereas the outer half was still composed of undifferentiated progenitor cells, as shown by the restricted expression of the early neural marker βIII-tubulin in the inner half (Fig. 2A). In Dicer-CKO mice, although the βIII-tubulin signal was observed in the inner side of the Dicer-CKO retina, there were also signals in the outer half of the retina; consequently, there was no clear boundary between βIII-tubulin–positive and -negative fields, as seen in the controls (Fig. 2A). Then we examined the expression of differentiation markers. GS, a marker of Müller glia cells, was expressed in the inner half of the retina in controls (Fig. 2A). Again, like the βIII-tubulin staining pattern, GS expression was scattered throughout the Dicer-CKO retina, and no boundary between GS-positive and -negative regions was observed. HuC/D, a marker for amacrine and ganglion cells, and Brn3b, which is expressed in ganglion cells, were expressed in the innermost part of the control retina, forming a layer-like structure (Fig. 2B). In the Dicer-CKO retina, HuC/D was weakly expressed with relatively stronger intensity in the inner half of the retina (Fig. 2B). The Brn3b pattern was also expressed in the inner side, and strong signals were also observed in the outer region (Fig. 2C). Although Brn3-positive cells were seen in the innermost side of the retina, the IPL was not observed, suggesting that process extension is inhibited by the depletion of Dicer. These results indicate that, in Dicer-CKO mice, early differentiation of retinal progenitor cells was under way. We next examined the time course of the expression of several markers. Expression of calbindin, an amacrine and horizontal cell marker, was clearly observed as making lines in the outer region and GCL at E19 in controls (Fig. 2D, blue arrows). In the Dicer-CKO retina, expression of calbindin was observed, but positive cells did not make lines and were scattered in the whole area of the retina (Fig. 2D). At P1, controls showed an expression pattern similar to that at E19, but in Dicer-CKO retina, the expression of calbindin was diminished (Fig. 2D).

Brn3 was expressed in GCL at all examined stages in control retinas. At E17 and E18, Brn3 signals were observed at the innermost side of the retina, and it was also scattered at all areas of the retina. At later stages, the number of positive cells decreased, but signals were observed in all areas of the retina (Fig. 3A). We counted the Brn3-positive cells semiquantitatively, and the cell numbers of Brn3 were slightly fewer in

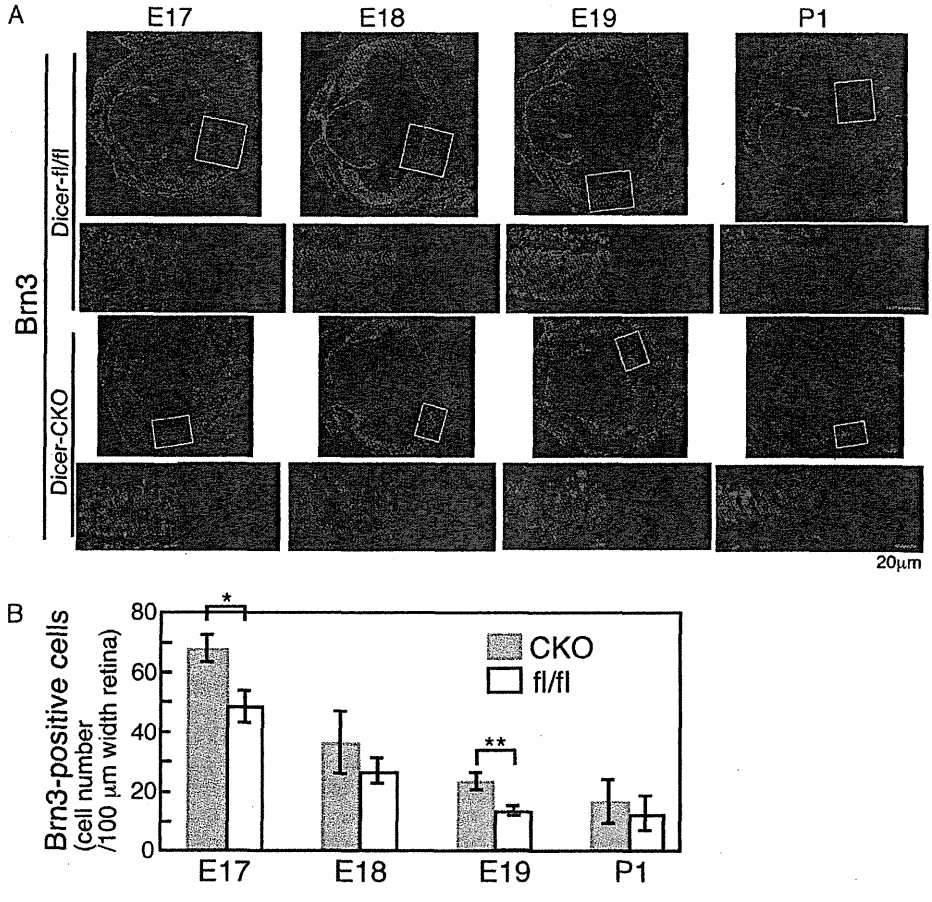

FIGURE 3. Enhanced expression of Brn3 in developing retinas of Dicer-CKO mice. (**A**) Retinas from Dicer-CKO or littermate control mice at indicated stages were frozen sectioned. Immunostaining using anti-Brn3 antibody was performed, and nuclei were visualized by DAPI staining. Scale bars, 100 μm. *Lower* panels are enlarged images of the *white squared regions* in the *upper* panels. (**B**) The number of Brn3-positive cells in the retina at indicated stages was examined. Brn3-positive cells at the central region of the retina were counted under a microscope in an area 100-μm wide. The average of three independent retinas with SD is shown. $^{**}P < 0.01$ and $^{*}P < 0.05$, were calculated by Student's *t*-test.